Bi-directional Low Pass Filter and Mixer Design

By

Meshach Milon Paul Pears Pradeep Kumar (me5254pa-s)

and

Sharath Thandava Murthy (sh5402th-s)

Department of Electrical and Information Technology
Faculty of Engineering, LTH, Lund University
SE-221 00 Lund, Sweden

Supervisor : Henrik Sjöland (LTH)

Ufuk Özdemir (Ericsson)

Kirill Kozmin (Ericsson)

Examiner: Pietro Andreani (LTH)

LUND UNIVERSITY

ERICSSON

2020

Abstract

This report presents the research and implementation of a bidirectional filter and mixer combination for the transceiver chain in 5G TDD equipment. The main objective of this project is to find a feasible design for mixer and low pass filter to reuse the same hardware blocks for both transmitter and receiver chain. The reuse of the hardware blocks effectively reduces the area, power consumption, and routing complexity of the system. A bidirectional low pass filter incorporating transconductor based active inductors are presented in this work. This choice is due to the Gm-C-based inductor's performance metric in the sub-gigahertz to the gigahertz frequency range. The voltage mode passive mixer is used for frequency up and down-conversion in transmit and receive cases, respectively. This choice of the mixer has reduced power consumption and integration complexity. The simulation results show that the filter frequency response has a sharp roll-off at $1.2GHz$ and an attenuation of $40dB$ at $3.2GHz$, and a passband gain of $-0.8dB$ and $-0.7dB$, respectively for transmitting and receiving case. For the transmitter chain, the measured overall voltage gain is $-5.749dB$, and the OIP3 is $-10.7dBm$. For the receiver chain, the overall voltage gain is $-8.085dB$, and IIP3 is $2.08dBm$.

Acknowledgments

First and foremost we would like to express our gratitude towards our supervisor Henrik Sjöland, Ufuk Özdemir, Kirill Kozmin, as well as our examiner Pietro Andreani, for their support and guidance throughout this thesis. We would like to show our gratitude to Rikard Gannedahl who helped us when we had doubts about RF concepts. We would like to express our gratitude towards Torbjörn Olsson and Ericsson, Lund for providing us the opportunity and letting us carry out our project with them. Lastly, we would like to express our gratitude towards LTH for providing us the opportunity to educate ourselves.

I, Meshach Milon, would like to express my gratitude towards all the people that have been by my side during my education. All my co-students and friends who have supported me during my studies and that have provided me with everlasting memories. I would like to thank Sharath for doing this project with me, he has been both resourceful and helpful, and it was nice to have someone to discuss with and to learn from. Especially, I would like to thank my family for always being there for me and providing me with the love and energy to carry on.

I, Sharath Thandava Murthy, would like to express my gratitude towards all people being supportive of me during my master's studies at Lund University. Thank you, Meshach Milon, for being a compatible work partner sharing your knowledge and time. It was my pleasure to work with such a good co-student who is interactive and open-minded. I would like to thank my parents and brother for being the backbone and supporting me in all the way possible with their love and care. I would like to especially thank my fiancé for being the greatest support and being with me in every thick and thin. I would also like to thank all my friends who have helped me thrive in my Master's.

Contents

List of figures

List of tables

Popular Science Summary

The internet has become an essential part of life and the number of internet users increases rapidly; and the internet is no more just used to search for information as it was in the past. The emerging technology trends have paved the way for use of the internet in various applications like the Internet of Things (IOT's) automated vehicles, smart wearables to keep track of daily activities; these applications are made possible with high-speed data connectivity and smaller devices for better mobility. The evolution of wireless standards to 5G (fifth generation) provides high-speed data connectivity. At the same time, there is a goal to reduce the overall power consumption of the base stations. This can be achieved partly by moving from a discreet component to IC (integrated circuits) designs and partly by using transceiver low power topologies. This work presents one such topology which makes the transceiver bidirectional, thus reducing its size and power consumption. In a conventional transceiver chain, separate blocks for transmitting and receiving a signal are used this is because of Frequency Division Duplexing (FDD) of operation and strict RF specifications in previous generations of wireless standards, but in 5G (fifth-generation) the mode of operation is Time Division Duplexing (TDD) and have relaxed radio frequency (RF) specifications. Hence there is a possibility of using the same hardware blocks for transmitter (Tx) and receiver (Rx) mode of operation. Thus, the chip areas can be significantly reduced. Since the number of blocks is also reduced the overall power consumption in a transceiver chain is reduced as well. The main building blocks in a transceiver chain are a filter that is used for removing undesired signals, a mixer which is used to perform frequency translation, a Low Noise Amplifier (LNA) to amplify a received signal, and a Power Amplifier (PA) to amplify a transmitting signal. The filter and mixer blocks are used both in the transmitting and receiving chain whereas LNA is used in the receiver and PA used in the transmitter blocks. The proposed design idea is to make the filter bidirectional hence we can use a single filter that provides necessary filtering in both Tx and Rx case, this is done by selecting a bidirectional architecture for filter design. The mixer block is designed using a diode ring topology which is bidirectional by design. The future work is aimed to make LNA and PA bidirectional by integrating both their functionality in a single circuit block.

1. Introduction

Telecommunication technology advancement has opened the door for 5G, the next-generation cellular network technology. The new networks will have higher bandwidth, enabling faster download speeds, up to a maximum of 10 $Gbit/s$. With rising bandwidth, new networks should not only serve mobile telephones such as existing mobile networks but also be used as general internet service providers for laptops and desktop computers, competing with existing cable network ISPs, as well as allowing new IoT and M2M applications to develop. The new networks can't use existing 4G technology, which requires 5G enabled wireless devices. This work presents a novel approach to reduce the area and power consumption by reusing the same blocks for transmitter and receiver, i.e. to make components work in a bidirectional mode of operation. The FDSOI 22nm technology process design kit (PDK) is used for design and simulation.

2. Analog Filter

2.1. Introduction

A filter is a circuit capable of passing (or amplifying) certain frequencies while attenuating other frequencies. Filters are used in electronics and telecommunication, in radio, television, audio recording, radar, control systems, music synthesis, image processing, and computer graphics. Ideally, a filter can extract important frequencies from signals that also contain undesirable or irrelevant frequencies as shown in Fig. 1. These signals might be continuous(analog) or discrete(digital) depending on application. We reject frequency components of a signal by designing a circuit that attenuates the band of frequencies and retains only the desired components of the signal. Such circuitry is known as filters.

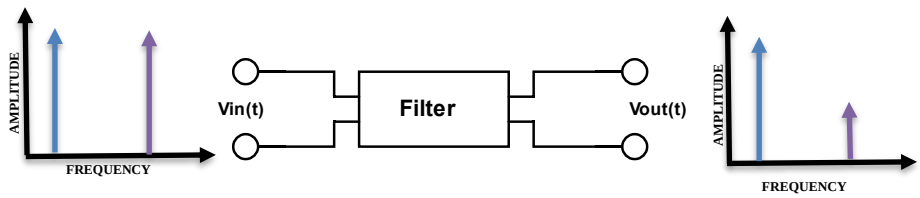

Fig. 1. Using the filter to reduce the effect of the undesired signal.

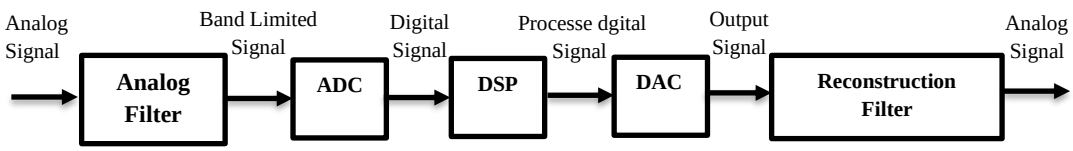

Fig. 2. Signal Processing Scheme.

As shown in Fig. 2 the analog filter is used to process the analog input signal to obtain a band-limited signal which is then sent to the Analog to Digital converter block for further processing. Since the analog signals are continuous-time signals and contain an infinite number of points it becomes almost impossible to digitize an infinite number of points as it required an infinite amount of memory to process the data. This issue can be mitigated by sampling the analog signal to a finite number of points with a fixed time interval as shown in Fig. 3.

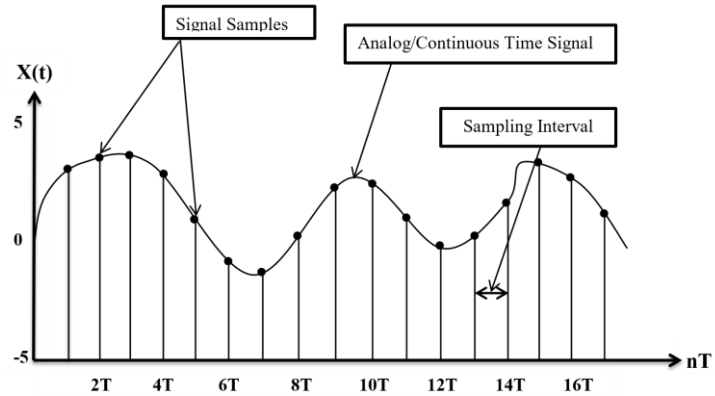

Fig. 3. A sampling of Analog Signal [6].

For a given time interval T between two samples the sampling frequency is defined as

$$F_s = \frac{1}{T}\, Samples\ per\ second(Hz). \tag{1}$$

To ensure that the samples are collected at a higher rate so that the original signal can be reconstructed at a later stage the sampling frequency is set to be twice the maximum frequency of the signal. If a signal is not properly sampled it will lead to aliasing which will introduce unwanted signals in the desired band.

This is stated by the Shannon sampling theorem which guarantees that the analog signal can be perfectly reconstructed if the sampling frequency is twice the highest frequency component of the signal.

$$F_s \geq 2F_{max}. \tag{2}$$

The sampled data when processed by a DSP system may result in a spectrum consisting of scaled baseband spectrum at origin and its replicas centered at $\pm nF_s$ $(n = 1,2,3,4 \dots \dots \dots)$[6].

In practice, anti-aliasing LPF will be employed before sampling to remove a higher frequency component which causes aliasing, and an anti-imaging LPF filter will be applied after the DAC to smooth the recovered sampled signal and to reject the image components.

2.2. Transfer Function

As filters are defined by their frequency-domain effects on signals, analytical and graphical descriptions of filters are represented and evaluated in the frequency domain. Thus, curves of gain versus frequency and phase versus frequency are commonly used to illustrate filter characteristics are in the frequency domain.

The transfer function is the mathematical representation of filter behavior in the frequency domain. It is the ratio of the Laplace transforms of its output and input signals. Fig. 4 shows a two-port network with a voltage source $V_{in}(t)$ connected to the source terminal 1-1´ and the output voltage $V_{out}(t)$ at the output terminal 2-2´.

Fig. 4. Two-port network floating input and output ports.

The voltage transfer function can be written as (3).

$$T(s) = \frac{output\ quantity}{input\ quantity} = \frac{V_{out}(s)}{V_{in}(s)} \tag{3}$$

The transfer function defines the filter's response to any arbitrary input signals, but we are most often concerned with effects on continuous sine waves, especially the magnitude of the transfer function to signals at various frequencies. Knowing the transfer function magnitude at each frequency allows us to determine how the filter can distinguish between signals at different frequencies. The transfer function magnitude versus frequency is called amplitude response or frequency response. Similarly, the phase response is the phase shift in the sinusoidal signal as a function of frequency.

By replacing the variables s in the (3) with $j\omega$, where $j = \sqrt{-1}$, and $\omega = 2\pi f$, we can find a filter effect on the magnitude and phase of the input signal. The magnitude is found by taking the absolute value of (3) as

$$|T(j\omega)| = \left|\frac{V_o(j\omega)}{V_i(j\omega)}\right|, \tag{4}$$

Or

$$\alpha(\omega) = 20\log|T(j\omega)| \; in \; dB. \tag{5}$$

And the phase is (6).

$$\theta(\omega) = \; \theta_o(\omega) - \theta_i(\omega). \tag{6}$$

2.3. Poles and Zeros

The transfer function provides the filter response as explained in section 2.2. As defined, the transfer function is the rational function of the complex variable $s = \sigma + j\omega$, and depicted as (7).

$$T(s) = \frac{N(S)}{D(s)} = \frac{b_m s^m + b_{m-1}s^{m-1} + \cdots + b_1 s + b_0}{a_n s^n + a_{n-1}s^{n-1} + \cdots + a_1 s + a_0} \tag{7}$$

It is often convenient to factorize the numerator and denominator and to write the transfer function in terms of those factors (8).

$$T(s) = \frac{N(S)}{D(s)} = \frac{(s - z_1) + (s - z_2) + (s - z_3) \ldots (s - z_{m-1}) + (s - z_m)}{(s - p_1) + (s - p_2) + (s - p_3) \ldots (s - zp_{n-1}) + (s - p_n)} \tag{8}$$

As written in (8) the $z_i's$ are the roots of the equation $N(S) = 0$, and are defined as the $zeros$, and the $p_i's$ are the roots of the equation $D(S) = 0$, and are defined to be the $poles$. All coefficients of polynomials $N(S) = 0$

and $D(S)$ are real. Therefore, the poles and zeros must either be real or complex conjugate pairs.

2.3.1. Pole-Zero Plot

The poles and zeros of the transfer function are represented graphically by plotting their locations on the complex $s-plane$, where the horizontal axis is σ (real axis) and the vertical axis is ω (imaginary axis). Such plots are known as $pole-zero\ plots$. It is usual to mark a zero location by a circle (o) and a pole location by a cross (×). The location of the poles and zeros provide qualitative insights into the response characteristics of a system. Fig. 5 shows an example of the pole-zero plot.

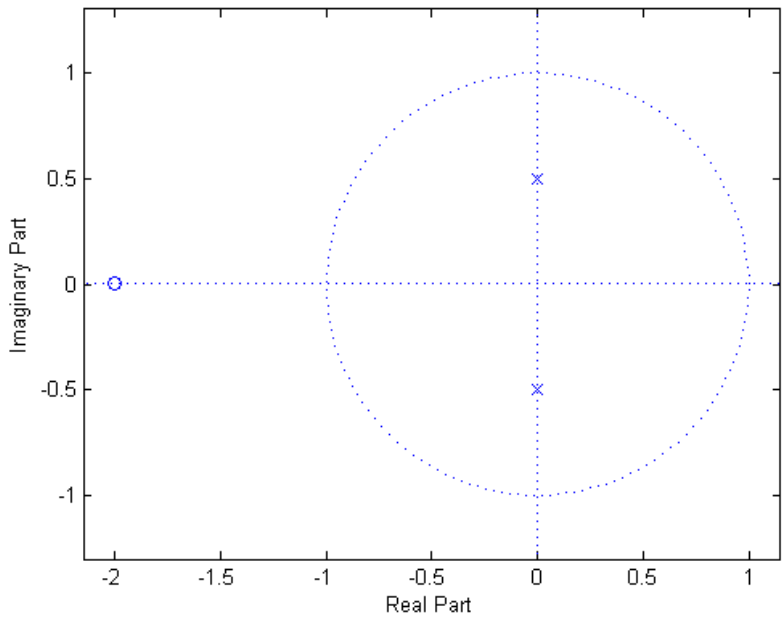

Fig. 5. Pole-Zero Plot [13].

The degree of the denominator is the order of the filter. Solving for the roots determines the poles and zeros. Each pole provides a $-6dB/Octave$ or $-20dB/decade$ response. Each zero will provide $+6dB/octave$ or $+20dB/decade$ response.

2.4. Basic Filter Types

Filters may be majorly classified as passive and active filters. Passive filters consist of a network of resistors, capacitors, and inductors. Despite the significant advantage of lower electrical noise, better signal to noise ratio (SNR) and better dynamic range passive inductors are found to be troublesome at higher frequencies as their size cannot be reduced to a level compatible with the modern integrated electronic circuit. Active filters on other hand avoid the use of inductors by having access to gain. It is comprised of passive components capacitors and/or resistors and the gain stage designed using operational amplifiers (OPAMPs) or operational transconductance amplifiers (OTAs)[1].

This chapter describes the basics of filters, different topologies, and in detail the description of Butterworth filter topology.

Filters can be classified as they perform in a different range of frequencies, as pass bands and stop bands. Ideally, the passband is such that $|T| = 1\ or\ \alpha = 0$, while in a stopband $|T| = 0\ or\ \alpha = -\infty$. The four most common filters are determined by the patterns of the passband and stopband. This is illustrated in Fig. 6 and defined as follows:

1. A *lowpass* filter has a passband from $\omega = 0\ to\ \omega = \omega_0$, where ω_0 is the cutoff frequency Fig. 6 (a).
2. A *high pass* filter is the opposite of a low pass filter in which the stopband range is from $\omega = 0\ to\ \omega = \omega_0$, while passband is from ω_0 to infinity Fig. 6 (b).
3. A *bandpass* filter is in which frequency band from $\omega_1 - \omega_2$ are passed while the others are attenuated to zero Fig. 6 (c).
4. A *stop-band* filter is the opposite of a bandpass filter where the frequencies from $\omega_1 - \omega_2$ are attenuated to zero and all other frequencies are passed Fig. 6 (d).

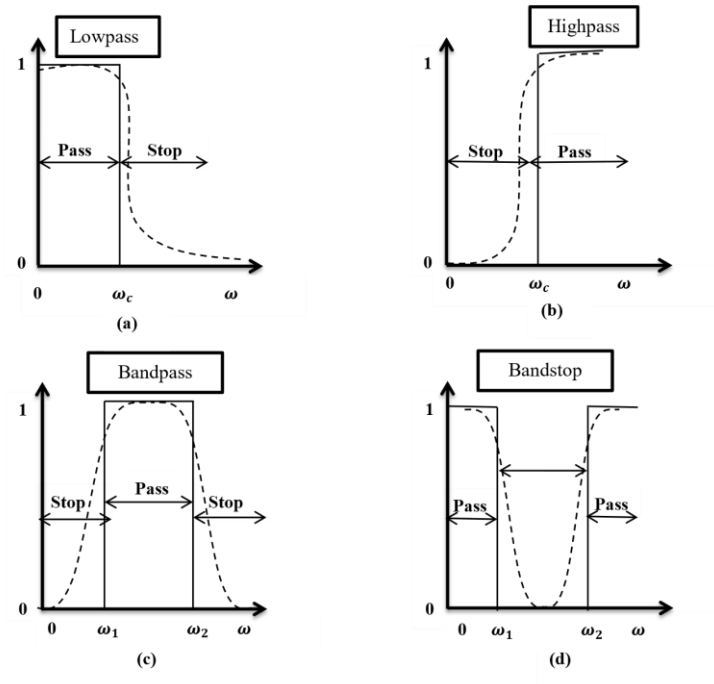

Fig. 6. The four basic types of filters [1].

It is not possible to realize the ideal transfer function as depicted in Fig. 6 with solid lines. Realistic filter characteristics are depicted by the dashed line in Fig. 6. Real filters are comprised of a finite number of elements and its transfer function is given by (9).

$$T(s) = \frac{N(S)}{D(s)} = \frac{b_m s^m + b_{m-1} s^{m-1} + \cdots + b_1 s + b_0}{a_n s^n + a_{n-1} s^{n-1} + \cdots + a_1 s + a_0} \tag{9}$$

- The numerator coefficients b_j can be positive, negative, or zero.
- The denominator coefficients a_i must be always positive.

If this restriction is violated the circuit will oscillate and transfer function cannot be realized with positive elements. Also, $n \geq$ m to be realizable with a finite number of real components.

2.5. Properties of Filter

Filter Order: It is directly related to the number of components in the filter, price, and complexity of the design. Higher the order of filter higher the price, area, and complexity of the filter. The key advantage of a higher-order filter is the steeper roll-off.

Roll-off rate: It is expressed as the magnitude of attenuation in dB over the range of frequencies. The most common units are "$dB/decade$" or "$dB/octave$".

From Fig. 7, four parameters are of concern:

- A_{max} is the maximum allowable change in the gain within the passband. This quantity is often called the maximum passband ripple.
- A_{min} is the minimum allowable attenuation within stopband.
- f_1 is the cutoff frequency of the passband limit.
- f_2 is the frequency at which the stopband begins.

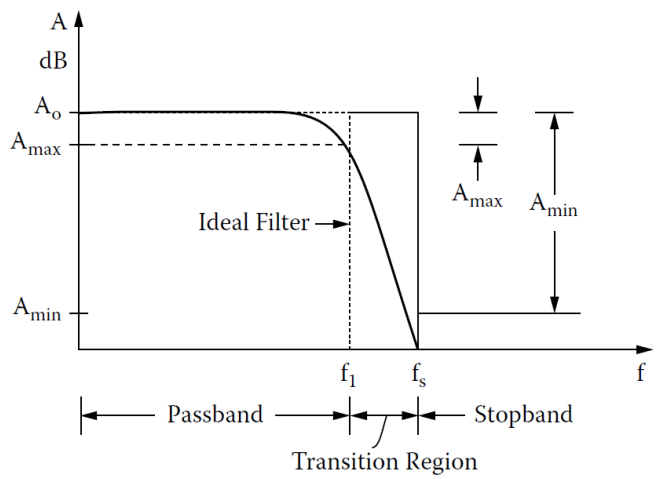

Fig. 7. The low pass filter response [2].

Q factor: A low pass filter may exhibit a resonant peak in the vicinity of the cut-off frequency, that is the gain can increase rapidly due to resonance effects. Q, the quality factor, represents the peakiness of this resonance peak, which is its height and narrowness around the cut-off frequency point.

In second-order filters, Q is represented by the damping factor ζ which is inverse of Q. The amplitude response of the second-order low pass filter varies for different values of damping factor, ζ. When $\zeta = 1$ or more the filter becomes "overdamped" with frequency response showing a long flat curve. When $\zeta = 0$, the filter output peaks sharply at the cutoff point resembling a sharp point at which the filter is said to be "underdamped". Then somewhere in between, $\zeta = 0$ and $\zeta = 2.0$, there must be a point where the frequency response is of the correct value, and there is. This is when the filter is "critically damped" and occurs when $\zeta = 0.7071$.

The second-order low pass filter is defined by the transfer function (10).

$$T(s) = \frac{{\omega_0}^2}{s^2 + \frac{\omega_o}{Q}s + {\omega_0}^2} \tag{10}$$

The amount of peaking for a second order low pass filter for different Q is shown in Fig. 8.

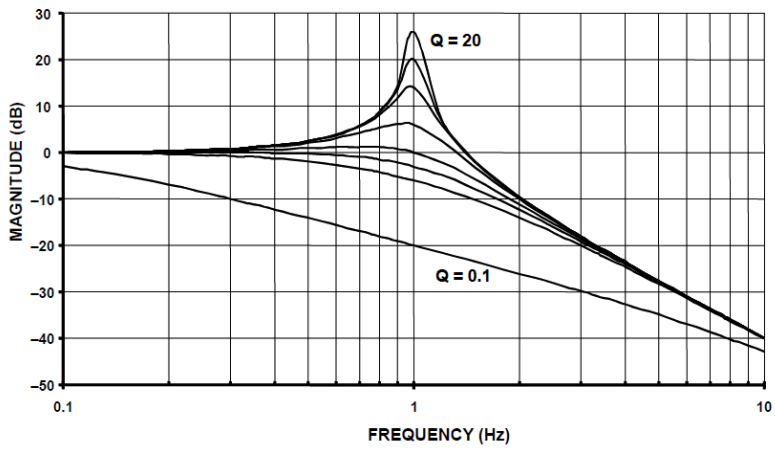

Fig. 8. Low pass filter peaking versus Q [1].

2.6. Why an Analog Filter?

As increasingly many filter applications are handled by digital signal and digital filters, there is always a debate on whether to use analog filters or digital filters for an application. There are numerous situations in which analog filters are either a necessity or provide an economical solution. Among these are interface circuits. These circuits are a bridge between the

real-world analog signals to the digital signal processor and provide band limiting before the signal is processed in the digital domain and reconstructed to analog signals. At high frequencies, ultrafast sampling and the digital circuitry are neither feasible nor economical [1] Fig. 9. Here analog techniques play a vital role.

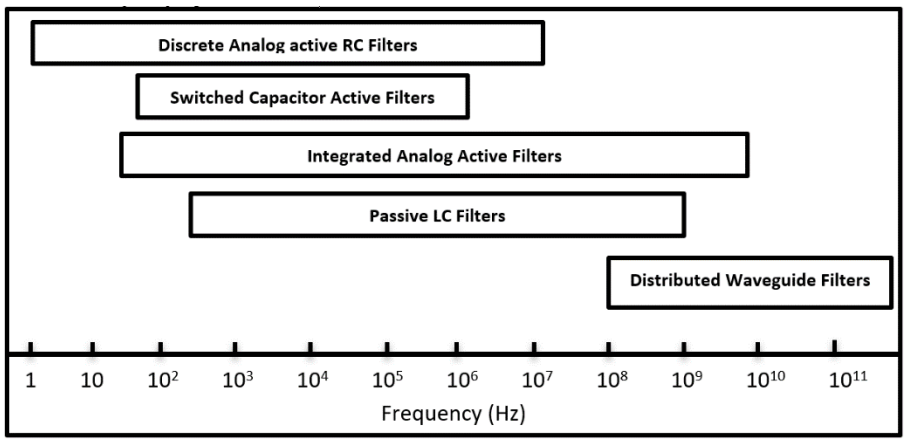

Fig. 9. The choice of filter types based on operating frequency [1].

Analog active filters use gain stage and capacitors. An integrated active filter gain is obtained by using opamps or operational transconductance amplifiers (OTAs), and we utilize capacitors and, resistors and at high frequencies, integrated inductors. To decide which components to use, we must consider factors such as the following:

1. The technology desired for system implementation.
2. Availability of dc supplies for active devices for power consumption.
3. Cost.
4. The range of frequency of operation.
5. The sensitivity of parameter changes and stability.
6. Weight and size of the implemented circuit.
7. Noise and dynamic range of the realized filter.

2.7. Different Filter Configuration

There are main factors considered while deciding the filter configuration some of them are:

- The frequency response in the passband.
- The transition from passband to stopband.
- The ability of the filter to pass the signal without any distortions within the passband.

In addition to these three the rising and falling time parameters also play an important role. By considering filters that satisfy some of all the factors they can be classified as Butterworth filter, Chebyshev filter, Bessel filter, and Elliptic filter.

2.7.1. Butterworth Filter

- This filter approximation is also known as the maximally flat response approximation as it provides the flat passband response Fig. 10.
- It does not have any ripple in the stopband and the roll-off rate is $20n\ dB\ /decade$. Where n is the order of the filter.
- It has a smooth transition at cutoff frequency because it has a quality factor of 0.707.
- The disadvantage of this configuration is that it has a wide transition band as it changes from passband to stopband.
- It is most often used in audio processing applications where flat passband response is necessary.
- Butterworth poles lie along a circle and are spaced at equal angular distances around a circle, but the horizontal distance between the poles and origin differs. Thus, poles have different Q values.

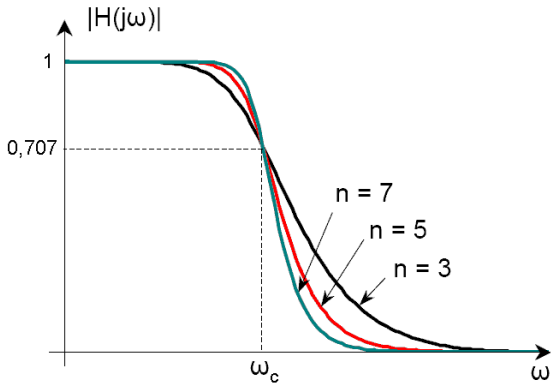

Fig. 10. Butterworth Filter response [3].

2.7.2. Chebyshev Filter

- The main aspect of the Chebyshev filter is that it has the steepest roll-off than Butterworth filter approximation Fig. 11.
- This property is vital to filter unwanted products with higher attenuation.
- Despite the steep roll-off, it has ripples either in the passband or stopband.

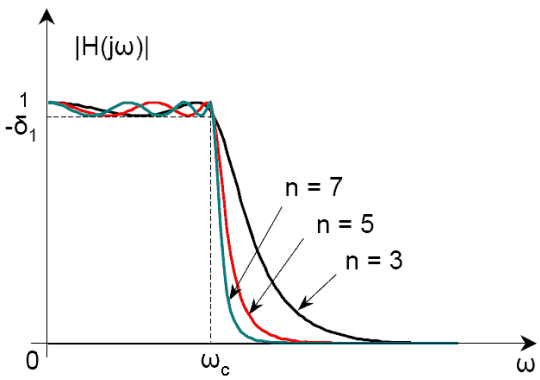

Fig. 11. Chebyshev Filter Response[3].

2.7.3. Elliptic Filter

- The elliptic filter is characterized by the ripple in both passband and stop-band Fig. 12.
- It has the fastest transition among all the filter approximations mentioned.
- It has a very poor step response.

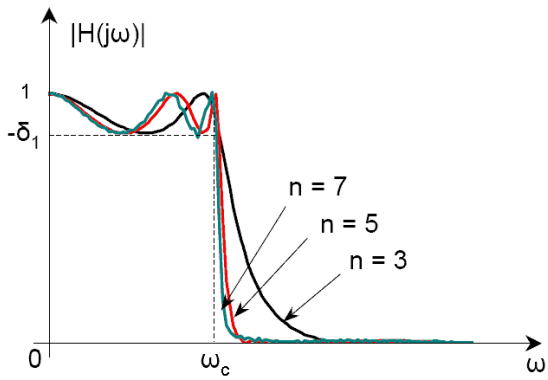

Fig. 12. Elliptical Filter Response[3].

2.8. Low Pass Butterworth Filter Design

Our thesis work has the following specifications to achieve as Table 1.

Table 1. Specifications.

Parameter	***Value***
$1dB\ Cut-Off\ Frequency$	$1.2GHz$
$Attenuation\ at\ 3.2GHz$	$35dB$

The major specification of our project is to have bidirectionality. As per the specification to achieve the $35dB$ attenuation at $3.2GHz$ we need to have a higher roll-off rate. Having the flat passband is advantageous to have equal gain for the signals below the cut off frequency. These specifications can be achieved easily by the Butterworth filter configuration, higher-order

filter increases the roll-off rate, maximal flat passband response of Butterworth filter configuration proves to advantageous and finally, the Cauer topology design of odd order Butterworth filters are bidirectional. These features of the Butterworth filter design are a promising approach for our project. Thus, in our thesis, we have opted for the higher-order Butterworth filter with Cauer topology. The design of the Butterworth filter, selection of the order, and topology discussion are made in sections 2.8.1 and 2.8.2.

2.8.1. Determining the order of the filter

The generalized frequency response of the n[th] order Butterworth filter is given by the (11).

$$H(j\omega) = \frac{1}{\sqrt{1 + \varepsilon^2 \left(\frac{f_s}{f_c}\right)^{2n}}}, \tag{11}$$

Where: n - order of the filter,

f_c – cutoff frequency,

f_s – stopband frequency, and

ε – is the maximum passband gain.

If A_{max} is defined at the cutoff frequency at $-3\ dB$ corner, then $\varepsilon = 1$.

The filter requirements from table 1 are as follows:

$\omega_s = 3.2GHz$, $\omega_p = 1.4\ GHz$, $A_{max} = -3dB$, $A_{min} = -32dB$

$$10^{-32/20} = \frac{10^{-3/20}}{\sqrt{1 + \left(\frac{3.2 \times 10^9}{1.4 \times 10^9}\right)^{2n}}}$$

$$0.02511 = \frac{0.707}{\sqrt{1 + 2.2857^{2n}}}$$

$$2.2857^{2n} = 793.3282$$

$$n = 4.03 \cong 5.$$

As per the above calculation, we have decided to proceed with the 5th order butter worth filter.

2.8.2. Topology

The most often used topology for a passive realization of the filter is Cauer topology and for an active realization is Sallen-key topology.

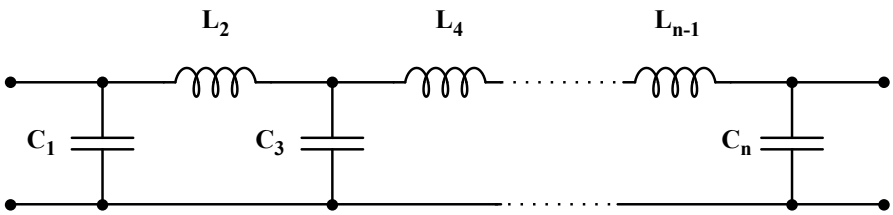

Fig. 13. Cauer topology[4].

[4] The Cauer topology uses passive components (shunt capacitors and series inductors) to implement the Butterworth filter as depicted in Fig. 13. The Butterworth filter having a given transfer function can be realized using a Cauer 1-form [4]. The kth element is given by (12) and (13).

$$C_k = 2\sin\left[\frac{(2k-1)}{2n}\pi\right] \; k = odd \tag{12}$$

$$L_k = 2\sin\left[\frac{(2k-1)}{2n}\pi\right] \; k = even \tag{13}$$

$$k = 1,2,3 \ldots n$$

Where n is the order of the filter.

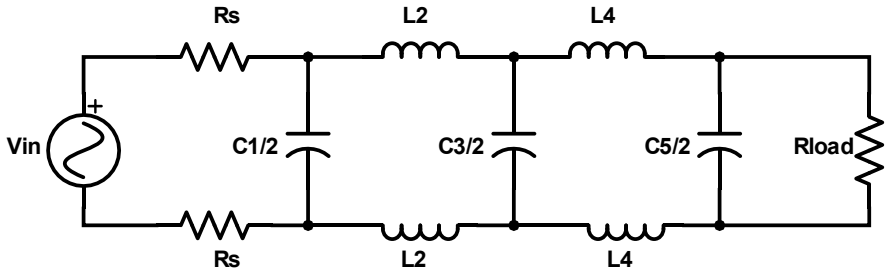

Fig. 14. Differential Passive Butterworth filter model.

The other important parameter that quantifies filter reliability is the pole-zero placements. The pole positions of the Butterworth filter are computed by (14).

$$-\sin\frac{(2k-1)\pi}{2n}+j\cos\frac{(2k-1)\pi}{2n}, \qquad k=1,2,\ldots,n \tag{14}$$

2.8.3. Passive design and results for Tx case

For the 5th order Butterworth filter, the normalized coefficients of LC elements are found by substituting the values of k and n in (12) and (13).

Table 2. Normalized LC values for $R_s = 100\Omega, R_{load} = 100\Omega$.

Order	C1	L2	C3	L4	C5
5	0.61803	1.61803	2	1.61803	0.61803

The terminal impedances of the filter are considered to determine the scaling of the LC component values from the normalized values and tabulated in Table 3.

Determining inductance (L):

$$L_k = \frac{R_s}{\omega_c} \times L_k(normalised). \tag{15}$$

Determining capacitance (C):

$$C_k = \frac{C_k(normalised)}{\omega_c \times R_s}. \tag{16}$$

Table 3. Determined LC values for Tx case.

Order	C1/2	L2	C3/2	L4	C5/2
5	351.25fF	18.394nH	1.137pF	18.394nH	351.25fF

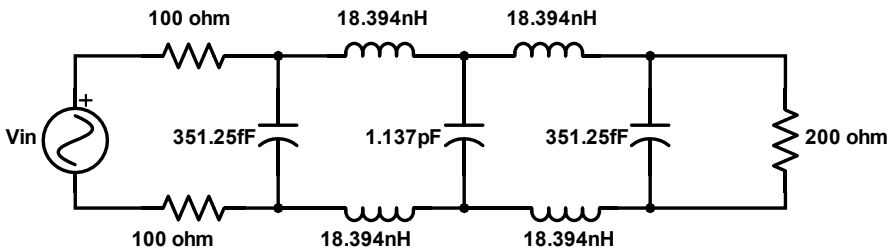

Fig. 15. Butterworth Filter LC component model for Tx case.

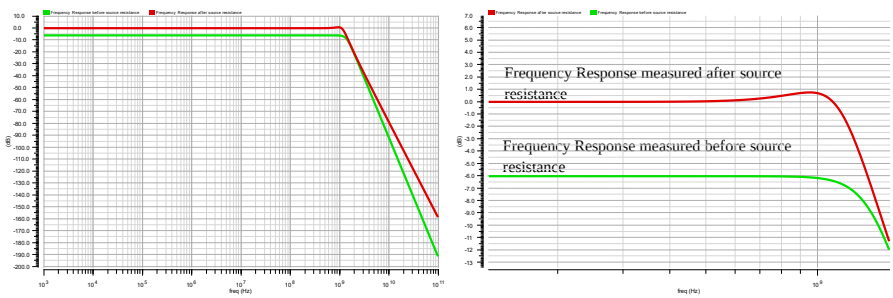

Fig. 16. Frequency response comparison at the different source point.

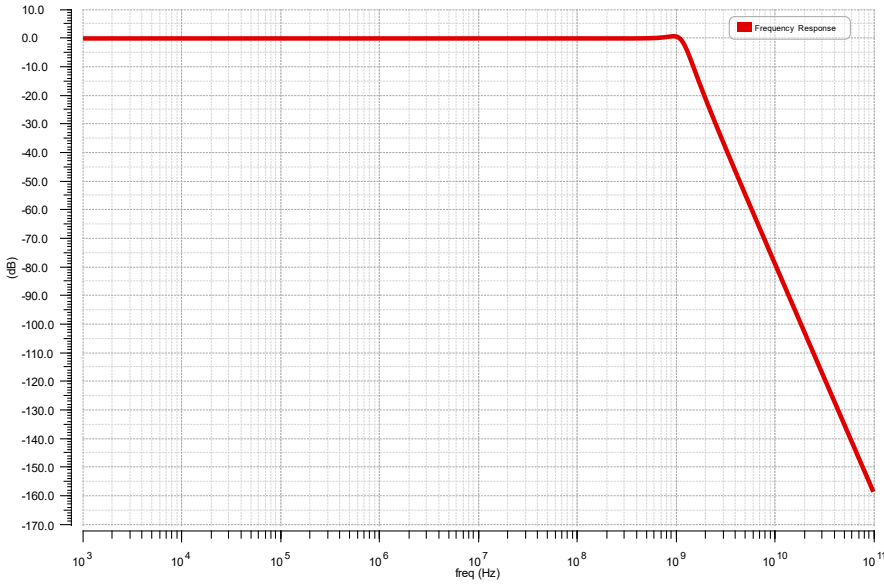

Fig. 17. Frequency Response.

As expected for the Butterworth filter configuration, Fig. 17 shows maximally flat passband and non-ripple stop-band.

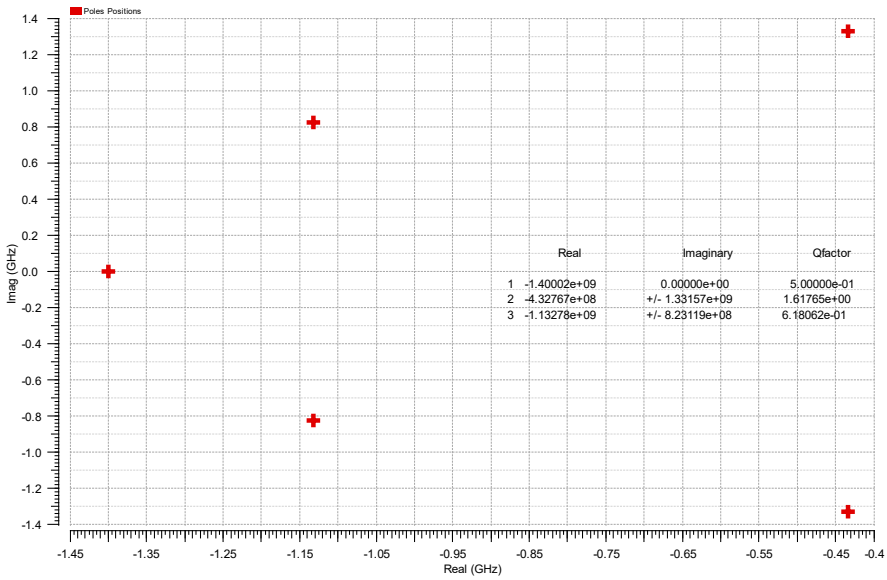

Fig. 18. Pole Position.

The equal angular spacing of the poles can be seen in Fig. 18. The poles positions and corresponding pole Q factor is mentioned in the plot.

2.8.4. Passive design and results for Rx case

For the 5th order Butterworth filter, the normalized coefficients of LC elements are found by substituting the values of k and n in (12) and (13).

Table 4. Normalized LC values for $R_s = 100\Omega, R_{load} = 100\Omega$.

Order	**C1**	**L2**	**C3**	**L4**	**C5**
5	0.61803	1.61803	2	1.61803	0.61803

The terminal impedances of the filter are considered to determine the scaling of the LC component values from the normalized values and tabulated in Table 5.

Determining inductance (L):

$$L_k = \frac{R_s}{\omega_c} \times L_k(normalised). \tag{17}$$

Determining Capacitance (C):

$$C_k = \frac{C_k(normalised)}{\omega_c \times R_s}. \tag{18}$$

Table 5. Determined LC values for Rx case.

Order	**C1/2**	**L2**	**C3/2**	**L4**	**C5/2**
5	351.25fF	18.394nH	1.137pF	18.394nH	351.25fF

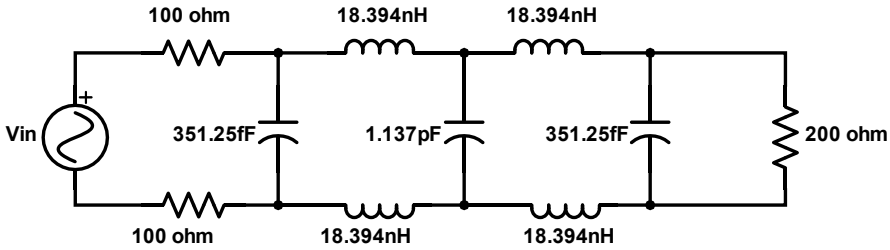

Fig. 19. Butterworth Filter LC component model for the Rx case.

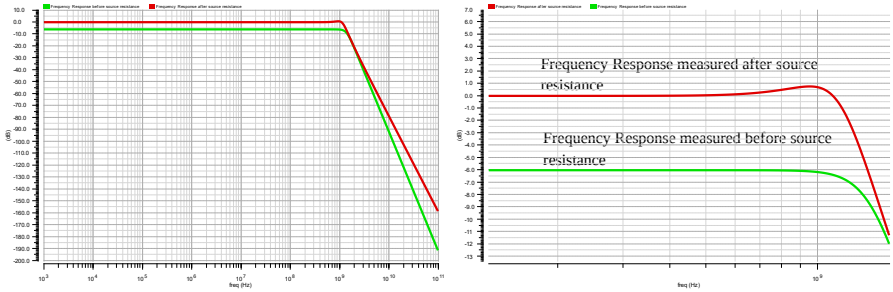

Fig. 20. Frequency response comparison at the different source point.

The frequency response in Fig. 16 and Fig. 20 shows the compared results of filter response measured at two different source impedance terminals. In the ideal case, the transfer-function is calculated including the source resistance to load resistance and we have a flat passband, but this resistance with shunt impedance act as a voltage divider and cause a loss in gain as shown there is the loss of $-7dB$. But in reality, the source for filter comes from a DAC (in case of Tx), and mixer (in case of Rx), and the input resistance of filter is seen from the output impedance of DAC and mixer respectively, so while measuring the response that resistance from DAC or mixer is not included which leads to a loss in a real pole which causes some passband ripples. Since the input resistance is not considered, we don't see any loss in a voltage gain of the filter.

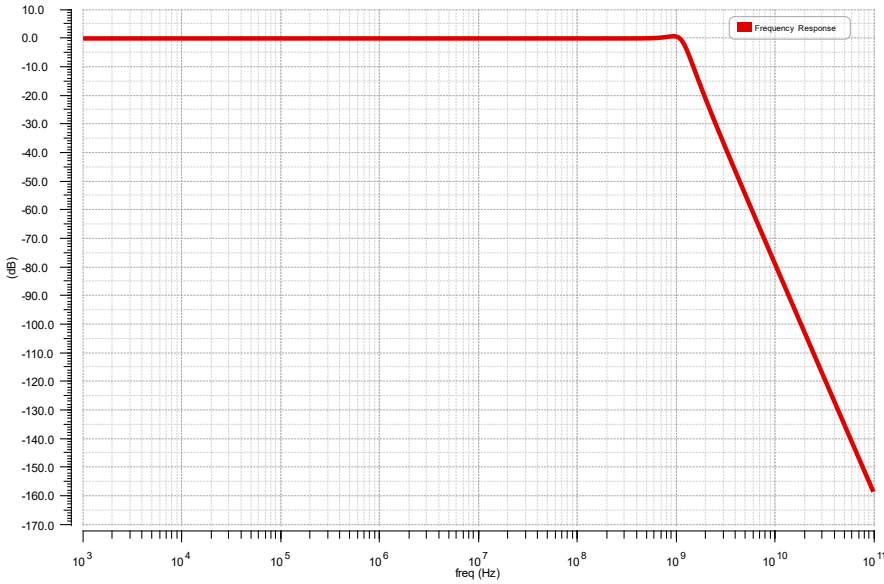

Fig. 21. Frequency Response.

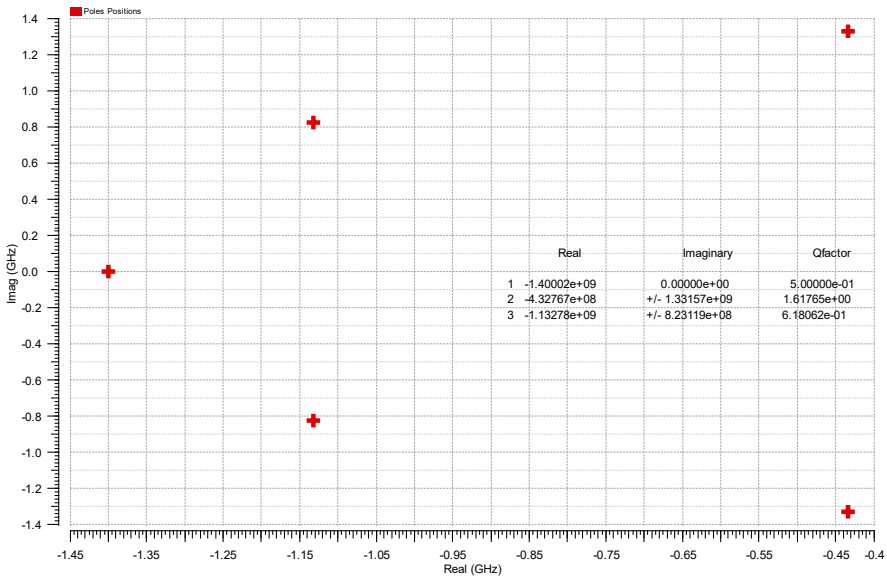

Fig. 22. Pole Position.

Both Rx and Tx cases have the same terminal impedances and this makes the response of Rx and Tx case to be identical and can be confirmed by comparing Fig. 21 & Fig. 22 along with Fig. 17 & Fig. 18.

3. Gm-C Filter

3.1. Gm Cell

The transconductance based approach for high-frequency filters can be designed using transistors which are voltage-to-current converters characterized by their transconductance parameter.

[1] The filters are designed using MOS transistors as it makes it feasible for our analog filters to be able to reside together with digital circuits on the same integrated circuit.

Fig. 23 shows the symbol and small-signal model of the MOS transistor. In the saturation region, the MOS transistor is governed by the equation (19).

$$i_D = \frac{1}{2}\mu C_{ox}\frac{W}{L}(v_{GS} - V_t)^2 \tag{19}$$

Here, the model's output current $i_o = i_D$ is the total drain current, i.e., the dc bias current I_D and the ac $i_d(t)$: $i_D = I_D + i_d(t)$. $v_{GS} = V_{GS} + v_{gs}(t)$ is the input gate-to-source voltage, μ is the carrier mobility, C_{ox} is the oxide capacitance per unit area of the channel, V_t is the threshold voltage, and W & L are the width and length of the gate. The transconductance of the device is defined as (20).

$$g_m = \frac{i_D}{v_{gs}} = \frac{\partial i_D}{\partial v_{GS}}\bigg|_{I_D, V_{GS}} = \frac{2I_D}{(v_{GS} - V_t)} = \sqrt{2\mu C_{ox}\frac{W}{L}I_D} \tag{20}$$

The g_m can be altered by the width-to-length ratio$\left(\frac{W}{L}\right)$, of the gate and is proportional to the square root of I_D.

MOS transistors are fundamentally voltage-controlled current sources characterized by transconductances. The bandwidth of the transistor is a few hundreds of megahertz and up to a few tens of gigahertz values.

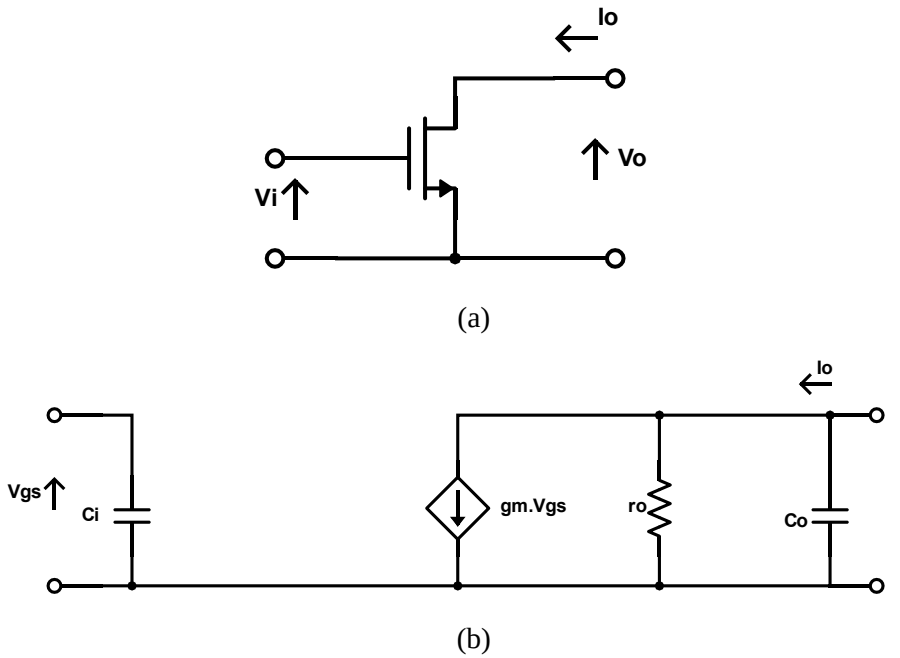

Fig. 23. MOS (a) symbol and (b) small-signal equivalent.

The practical transconductors are also referred to as operational transconductance amplifiers (OTAs). While developing the active filters using OTAs we must ensure that the transistors retain their high-frequency properties. The requirements like differential input and output, high output resistance increase the design complexity of the OTAs.

In analog integrated circuits, it is preferable to process signals differentially because of the following reasons:

- Differential processing has the advantage of better common-mode rejection, which helps to suppress external common-mode disturbances appearing in signal or supply paths.
- Active devices cause nonlinearities, these nonlinearities are canceled out in the differential pair.

To achieve differential input and differential output a simple differential common source amplifier with the PMOS common source load is used in the design as shown in Fig. 24. The PMOS transistors are self-biased by connecting the resistors to the gate of PMOS and between the drains of NMOS and PMOS. This also regulates the common-mode voltage at the desired design value.

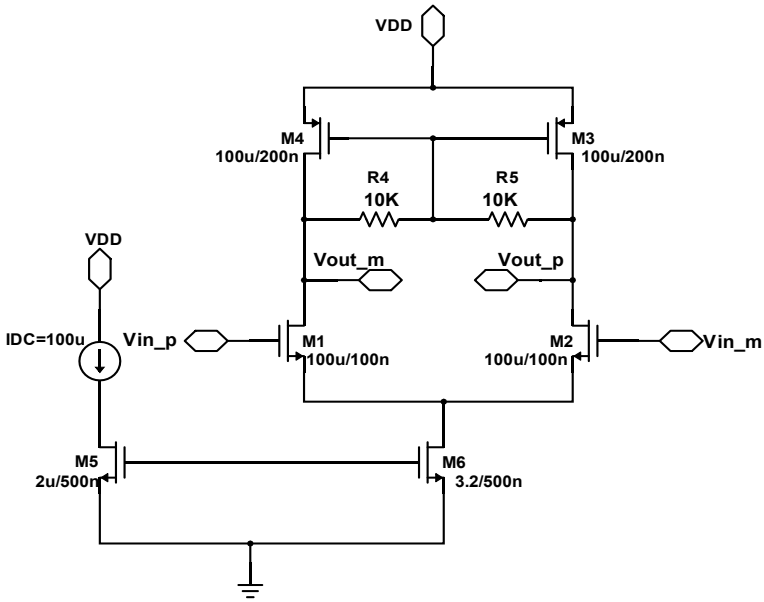

Fig. 24. g_m Cell Schematic.

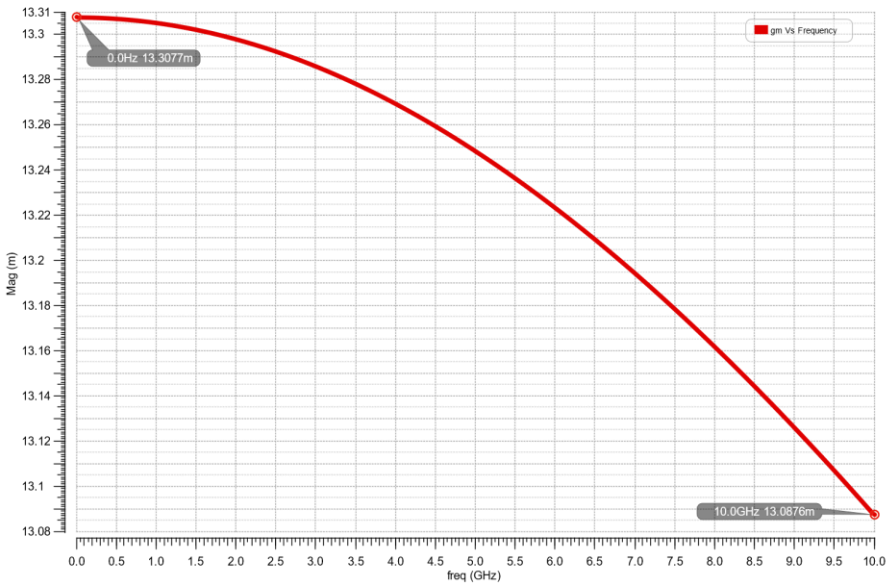

Fig. 25. g_m in mS across the frequency range 0-10 GHz.

Table 6. g_m Cell simulated parameters.

Parameter	Values
g_m	$13.31mS$
C_{in}	$83.44fF$
C_{out}	$58.73fF$
R_{out}	$5.432K\Omega$

Fig. 25 & Table 6 depicts the performance parameters of the designed g_m cell. As expected g_m cell has a large bandwidth, its g_m across the frequency up to $10GHz$ is simulated and found to be negligibly deviating from the g_m value at dc. The Table 6 gives insight of the small-signal parameters of the g_m simulated cell. These values form the parasitics in the design of active inductor which will be explained in the upcoming section 3.2.

3.2. Gm-C Inductor

3.2.1. Inductor

In wireless communication, capacitor and inductor are the most significant reactive components for frequency selection. Out of these two reactive components, the inductor requires the largest die area. As a result, any circuit containing a passive inductor such as voltage-controlled oscillator (VCO), low-noise amplifier (LNA), filter, and power dividers consume a relatively larger area than other blocks. To meet the requirement of microelectronics industries, passive components have been replaced with active ones.

3.2.2. Passive Inductor

An inductor is a two-terminal electrical device that stores energy in a magnetic field when an electric current flows through it. It stores electrical energy in the form of a magnetic field. The current passing through the inductor lags inductor voltage by 90°.

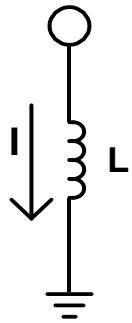

Fig. 26. Passive Inductor.

Current flowing through the ideal inductor as shown in Fig. 26 can be described by the equation (21).

$$Iin = (1/sL)Vin \tag{21}$$

$$Zin = Vin/Iin = sL \tag{22}$$

3.2.3. Active Inductor

The design of a tunable and compact RF-integrated circuit is challenging. Although spiral inductor is the common implementation approach in integrated circuits, it is possible to design active circuits. As reported in [7], active inductor occupies $1-5\%$ of the area passive inductor does and is tunable, unlike passive one.

Integrated circuits can be designed for a specific frequency and multiple frequency ranges. There are many methods to design active inductors but the most widely used approaches to design active inductors are:

1. Operational amplifier-based approach.
2. Gyrator-C-based approach.

The operational amplifier (op-Amp) based design is widely used at moderate frequencies (up to about $100\ MHz$). The latter one is the gyrator-C based approach, which can be operated from sub-gigahertz to gigahertz frequency range. Apart from the frequency limits, the op-amp-based circuit consumes a large silicon area and suffers from nonlinearity. As a

counterpart, the gyrator-based active inductor consumes a small chip area and has better linearity [7]. In the present work, to design an active inductor at $1.2GHz$ the gyrator-C-based active inductor approach has been considered.

3.3. Gyrator

An ideal gyrator is a linear two-port device that couples the current on one port to the voltage on the other port and vice versa. as shown in Fig. 27.

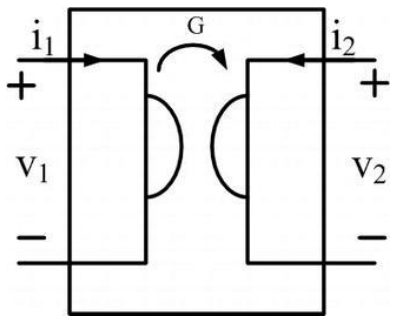

Fig. 27. Ideal gyrator.

The equation (23) and (24) shows the current through port 1 and port 2.

$$i_1 = G \times V_2 \times i_1 \tag{23}$$

$$i_2 = -G \times V_1 \times i_2 \tag{24}$$

where G is the conductance.

The conductance (G) relates the voltage on port 2 (V_2) to the current in port 1 (i_1). The voltage on port 1 (V_1) is associated with the current in port 2 (i_2), as minus shows the direction of conductance. It proves that the gyrator is a nonreciprocal device. From the gyration conductance, it is called a gyrator.

The ideal gyrator is described by the conductance matrix as shown below.

The impedance matrix is given by:

$$\begin{bmatrix} i_1 \\ i_2 \end{bmatrix} = \begin{bmatrix} 0 & G \\ -G & 0 \end{bmatrix} \begin{bmatrix} V_1 \\ V_2 \end{bmatrix} \tag{25}$$

$$Z = \begin{bmatrix} 0 & R \\ -R & 0 \end{bmatrix} \tag{26}$$

The admittance matrix is given by:

$$Y = \begin{bmatrix} 0 & G \\ -G & 0 \end{bmatrix} \tag{27}$$

The equivalent equations can be written as follows:

$$\begin{bmatrix} i_1 \\ i_2 \end{bmatrix} = \begin{bmatrix} 0 & Gm1 \\ -Gm2 & 0 \end{bmatrix} \begin{bmatrix} V_1 \\ V_2 \end{bmatrix} \tag{28}$$

The above matrix can result in a block diagram as illustrated in Fig. 28 it tells that gyrator comprises two transconductors: positive transconductor $Gm1$ and negative transconductor $Gm2$, connected in a closed-loop as shown in Fig. 28. The transconductor-1 shows positive transconductance means output current and input voltage are in phase. Whereas, transconductor-2 depicts negative transconductance means output current and input voltage are 180° phase-shifted.

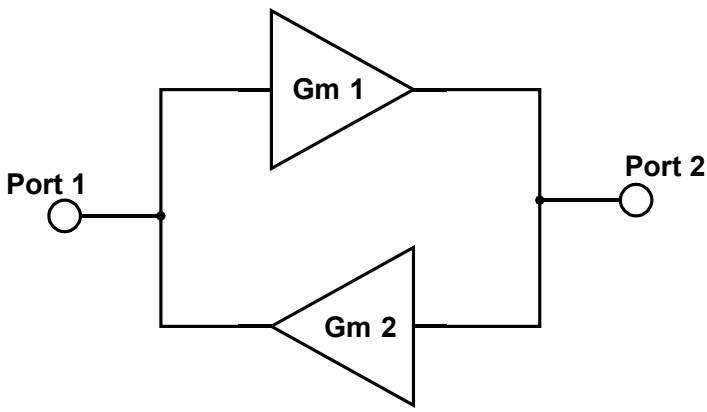

Fig. 28. Structure of gm gyrator.

3.3.1. Ideal Gyrator

When a capacitor is connected to the second terminal (port 2), an inductance is realized at the primary terminal (port 1) of the gyrator, which is entitled as gyrator-C topology, Fig. 29 shows the ideal single-ended gyrator-C structure, and Fig. 30 shows the gyrator structure for differential signals.

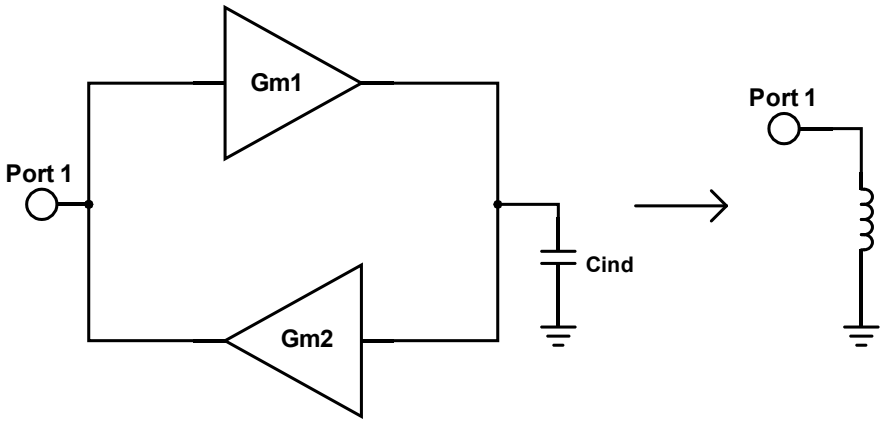

Fig. 29. Ideal gyrator-C based active inductor.

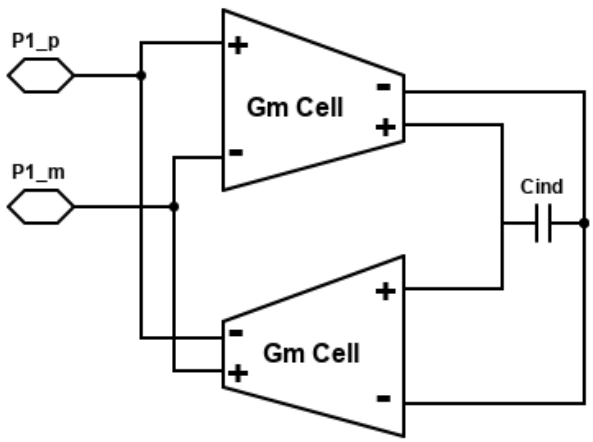

Fig. 30. Differential Gyrator Structure.

3.3.2. Gyrator-C-based Active Inductor and it's working principle

The equations tell us that input impedance Z_{in} is directly proportional to frequency, therefore is inductive. Subsequently, equivalent inductance can be defined as (30).

$$Z_{in} = \frac{V_{in}}{I_{in}} = \frac{sC}{G_{m1}G_{m2}} \tag{29}$$

$$L = \frac{C}{G_{m1}G_{m2}} \tag{30}$$

Therefore, the gyrator-C network can be used to synthesize active inductors. This synthesized inductor is called a gyrator-C active inductor.

In a practical active inductor circuit, along with the inductance, we do get parasitic components as series resistance R_S, parallel resistance r_o and parallel capacitance C_P as depicted in Fig. 31. These parasitic components affect the performance of the active inductor.

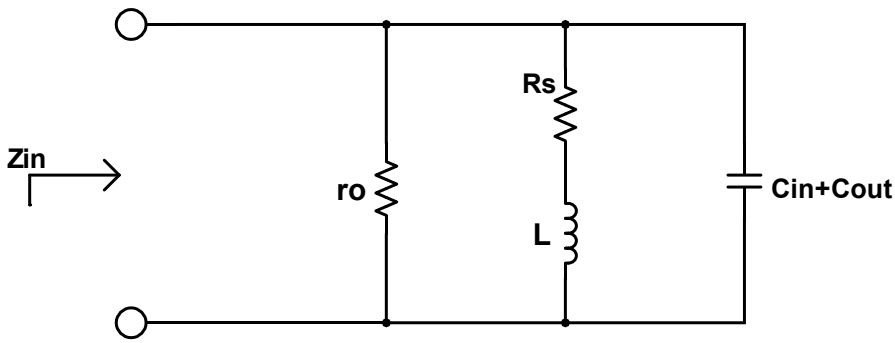

Fig. 31. Practical Inductor model.

3.4. Floating Active Inductor

The floating active inductor has a structure shown in Fig. 32, two unidirectional inductors connected back to back to form a bidirectional structure as shown in Fig. 32.

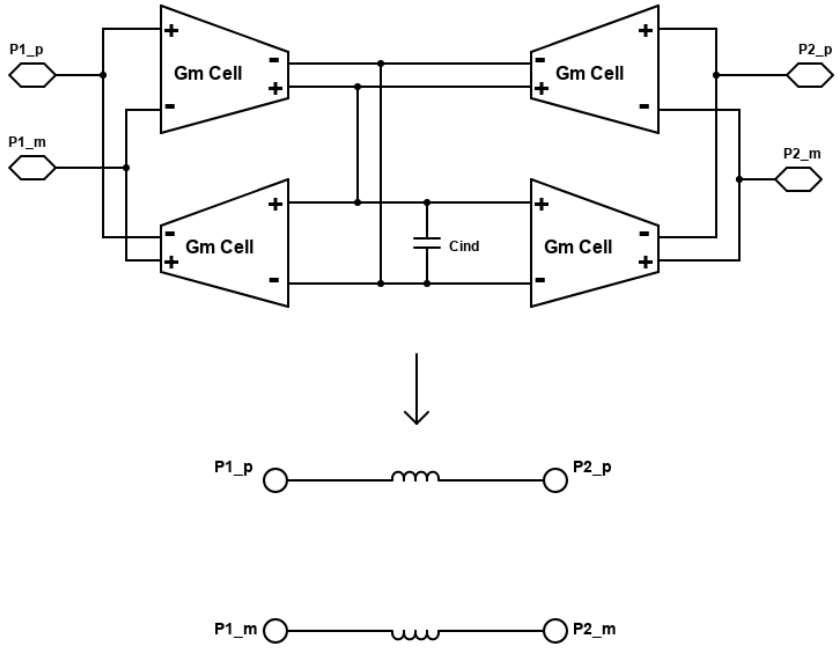

Fig. 32. Floating Inductor structure.

3.4.1. Performance Parameters of an Active Gm-C Inductor

An ideal inductor has a constant inductive behavior for the entire range of frequency, but a lossy active inductor has parasitics affecting its inductive performance range. The respective range can be analyzed by analyzing the equivalent RLC circuit as shown in Fig. 34 of the Gm-C active inductor.

To derive the active inductor parameters shown in Fig. 34, we need to draw the equivalent small-signal circuit of the Gm-C active inductor as in Fig. 33.

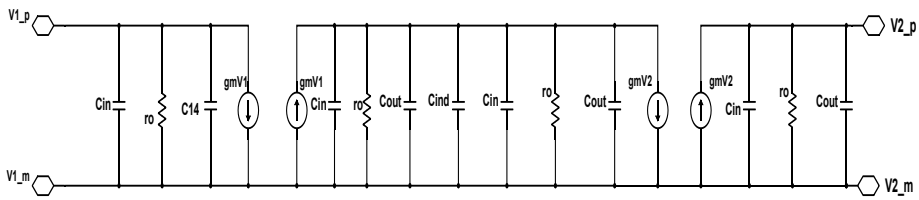

Fig. 33. The small-signal equivalent of the bidirectional inductor.

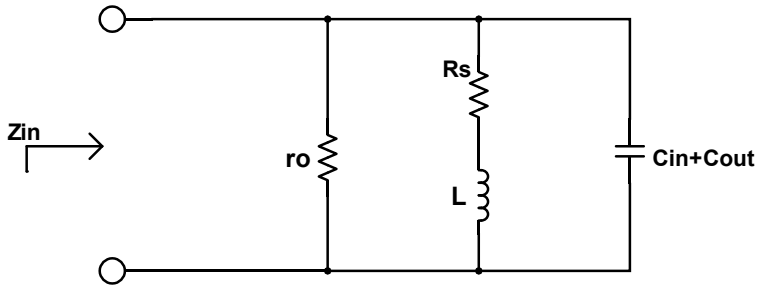

Fig. 34. Equivalent RLC circuit.

Where,

$$R_s = {}^{g_o}/_{g_{m1}g_{m2}}, \tag{31}$$

$$L = \frac{(C_{ind} + 2(C_{in} + C_{out}))}{(g_{m1}\, g_{m2})}, \tag{32}$$

$$C_p = C_{in} + C_{out}, \text{ and} \tag{33}$$

$$\mathrm{Z_{in}} = \left(\frac{R_S}{C_p L}\right) \frac{S\frac{L}{R_S+1}}{S^2+S\left(\frac{1}{R_p C_p}+\frac{R_S}{L}\right)+\frac{R_S+R_p}{R_p C_S L}}. \tag{34}$$

The inductive pole frequency of Z_{in} is given by (35).

$$\omega_p = \sqrt{\frac{R_p + R_s}{R_p C_p L}} \tag{35}$$

The quality factor is given by (37).

$$Q = \frac{I_m(Z_{in})}{R_e(Z_{in})} \tag{36}$$

$$Q = \left(\frac{\omega L}{R_s}\right) \frac{R_p}{R_p + R_s\left(1 + \left[\frac{\omega L}{R_s}\right]^2\right)} \left[1 - \frac{R_s^2 C_p}{L} - \omega^2 L C_p\right] \tag{37}$$

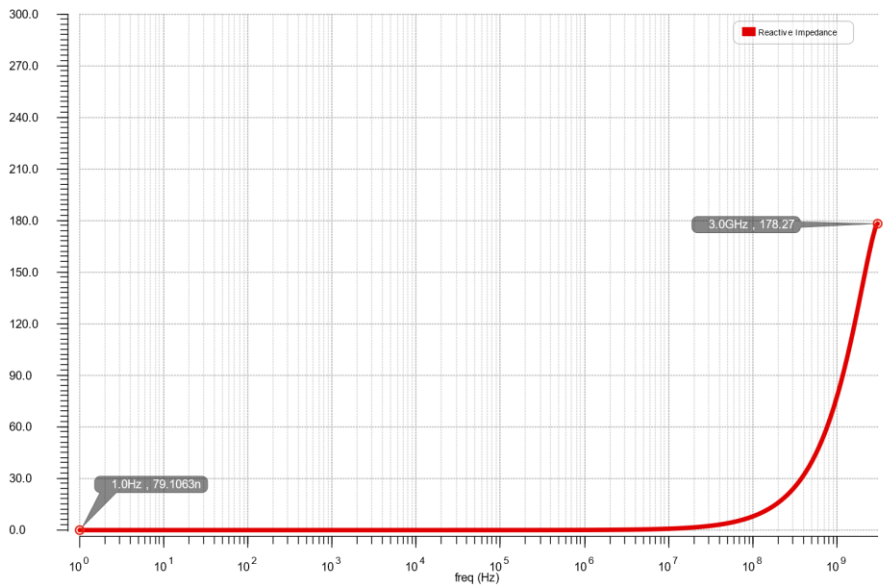

Fig. 35. Reactive Impedance as a function of frequency.

Table 7. Capacitance and its associated Inductance value.

$\boldsymbol{Cind}$ $(\boldsymbol{Theoretical})$	$\boldsymbol{Cind - 2(C_{in} + C_{out})}$	$\boldsymbol{Inductance(L)}$
$1629.2fF$	$1344.86fF$	$18.394nH$

Fig. 35 shows the reactive input impedance of the simulated Gm-C inductor. As can be seen, the reactive part of the input impedance should increase as the function of frequency, i.e., $X_L = 2\pi fL$ which denotes that reactive impedance is directly proportional to the frequency. This confirms the designed circuit behaves as an inductor. Table 7 tabulates the theoretical capacitance value and practical capacitance value after nullifying parasitic capacitances and corresponding inductance values used in the design of the Gm-C filter.

3.5. Gm-C Filter

The Gm-c filter is designed as shown in Fig. 36 by replacing the passive inductor based LPF design as explained in 2.8 by Gm-C based active inductor.

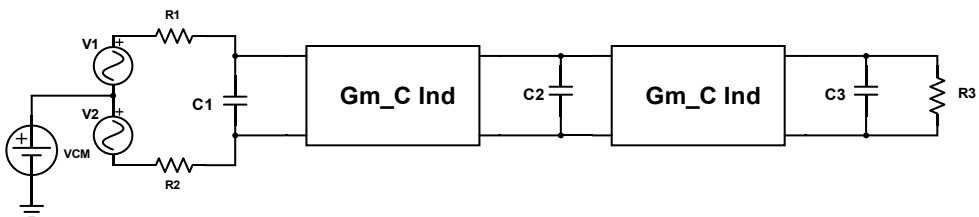

Fig. 36. Schematic of Gm-C based LPF.

Apart from the capacitances which form poles the parasitic capacitances associated with the Gm-C inductor add in parallel to the filter capacitances as shown in Fig. 37.

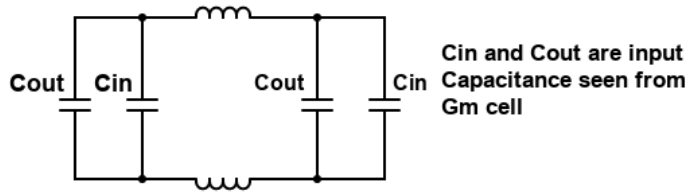

Fig. 37. Parasitic Capacitances associated with Gm-C Inductor.

The parasitic capacitances should be considered when calculating the values of filter capacitances C1-C3. See Table 8 to find associated parasitics and corrected values.

Table 8. Method to mitigate the effect of Parasitic Capacitances.

Filter Capacitances	$C1$	$C2$	$C3$
Parasitic Affecting	$C_{in} + C_{out}$	$2(C_{in} + C_{out})$	$C_{in} + C_{out}$
Effective Capacitance value	$C1 - (C_{in} + C_{out})$	$C1 - 2(C_{in} + C_{out})$	$C3 - (C_{in} + C_{out})$

3.5.1. LPF design for Tx case

Fig. 38 shows the schematic of LPF design using an active inductor, for the 5th order Butterworth filter, the normalized coefficients of LC elements are found by substituting the values of k and n (12) and (13) as explained in section 2.8.3.

The terminal impedances of the filter are considered to determine the scaling of the LC component values from the normalized values and tabulated in Table 10.

Table 9. Normalized LC values for $R_s = 100\Omega, R_{load} = 100\Omega$.

Order	**C1**	**L1**	**C2**	**L2**	**C3**
5	0.61803	1.61803	2	1.61803	0.61803

Determining Capacitance (C):

$$C = C - C_{Parasitic} \tag{38}$$

Table 10. Determined LC values for Tx case.

$Order$	$C1$	$L2$	$C2$	$L4$	$C3$
5	$209.08fF$	$18.394nH$	$852.66fF$	$18.394nH$	$209.08fF$

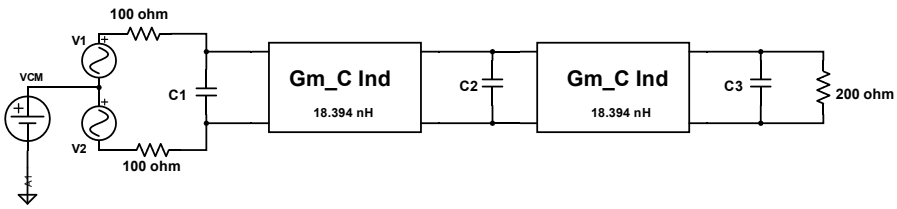

Fig. 38. Tx Chain LPF Schematic.

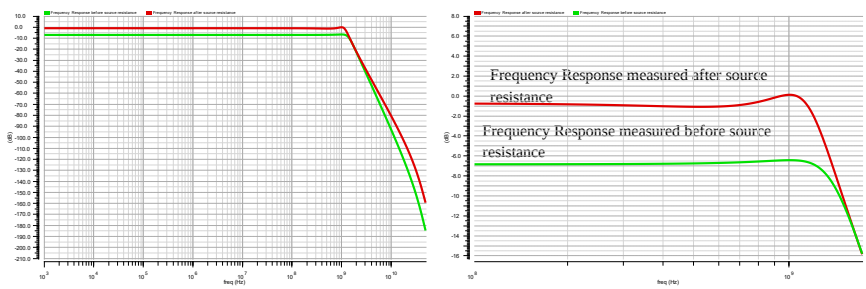

Fig. 39. Frequency response comparison at the different source point.

The frequency response in Fig. 39 shows the compared results of filter response measured at two different source terminals. In the ideal case, the transfer-function is calculated including the source resistance to load resistance and we have a flat passband, but this resistance with shunt impedance act as a voltage divider and cause a loss in gain as shown there is the loss of $-6.8dB$. But in reality, the source for filter comes from a DAC (in case of Tx), and the input resistance of filter is seen from the output impedance of DAC, so while measuring the response that resistance from DAC is not included which leads to a loss in a real pole which causes some

passband ripples. Since the input resistance is not considered, we don't see any loss in a voltage gain of the filter.

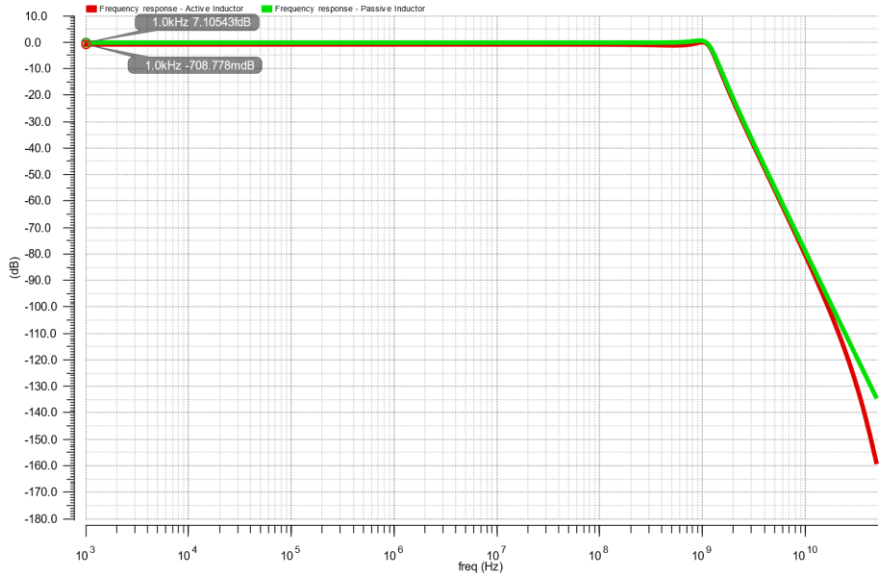

Fig. 40. The frequency response of Gm-C filter versus ideal filter.

The frequency response of the filter adopting $gm - C$ inductors is plotted and compared along with the filter response of the filter with a passive inductor (ideal) in Fig. 40, it can be seen that both filter responses are nearly identical. The gain of filter at $1KHz$ is marked in the plot.

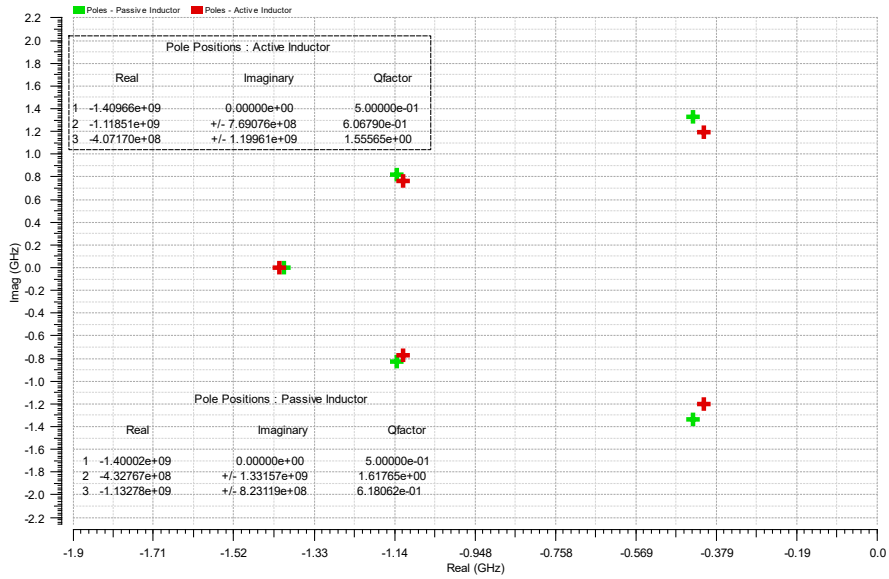

Fig. 41. The Pole position of Gm-C filter versus ideal filter.

The pole position of the filter adopting $gm - C$ inductors are plotted and compared along with the pole placement of the filter with a passive inductor (ideal) in Fig. 41, it can be seen that both have similar pole placements. The pole placement and their corresponding Q values are mentioned in the graph.

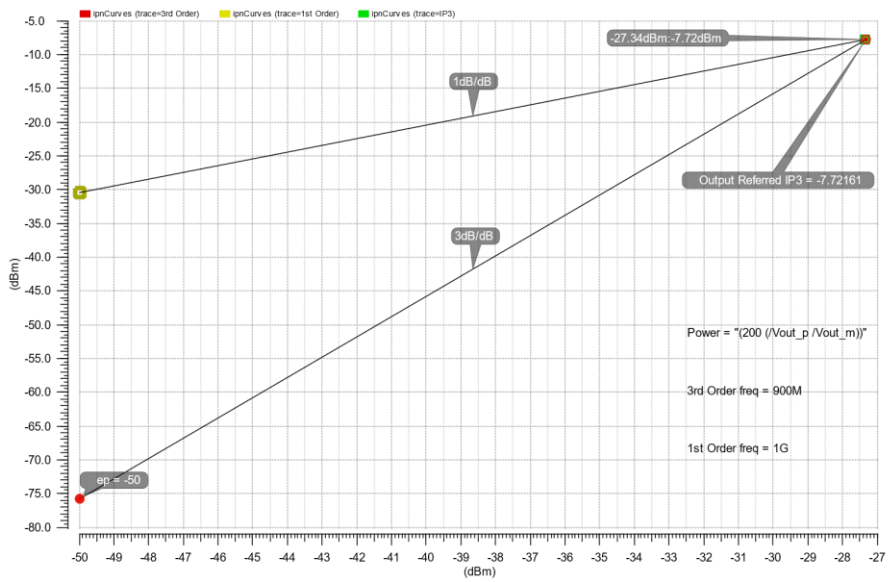

Fig. 42. Output referred IP3 of the Gm-C filter.

Table 11. Performance parameters Tx.

PARAMETERS	***VALUES***
IDC	$9.598mA$
$IDC\_indctuctor1$	$4.827mA$
$IDC\_indctuctor2$	$4.771mA$
VCM	$408.4mV$
VCM_in	$403.9mV$
VCM_mid	$407.6mV$
VCM_out	$407.7mV$
Av_Gain_dB	$-707mdB$
$1dB\ cutoff\ Frequency$	$1.186GHz$
$dB/Octave$	24.89
$Attenuation\ at\ 3.2GHz$	$32.45dB$

Table 11 shows the performance metric of the Tx case with parameter values close to the design specifications.

3.5.2. LPF design for Rx case

Fig. 43 shows the schematic of LPF design using an active inductor, for the 5th order Butterworth filter, the normalized coefficients of LC elements are found by substituting the values of k and n (12) and (13) as shown in section 2.8.3.

The terminal impedances of the filter are considered to determine the scaling of the LC component values from the normalized values and tabulated in Table 12.

Table 12. Normalized LC values for $R_s = 100\Omega, R_{load} = 100\Omega$.

Order	**C1**	**L1**	**C2**	**L2**	**C3**
5	0.61803	1.61803	2	1.61803	0.61803

The terminal impedances of the filter are considered to determine the scaling of the LC component values from the normalized values and tabulated in Table 13.

Determining Capacitance (C):

$$C = C - C_{Parasitic} \tag{39}$$

Table 13. Determined LC values for Rx case.

Order	C1	L2	C2	L4	C3
5	$209.08fF$	$18.394nH$	$852.66fF$	$18.394nH$	$209.08fF$

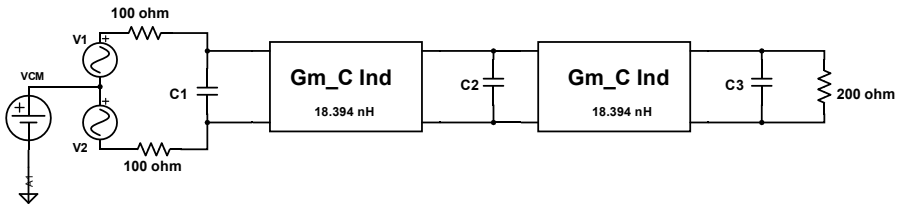

Fig. 43. Rx Case Gm-C filter Schematic.

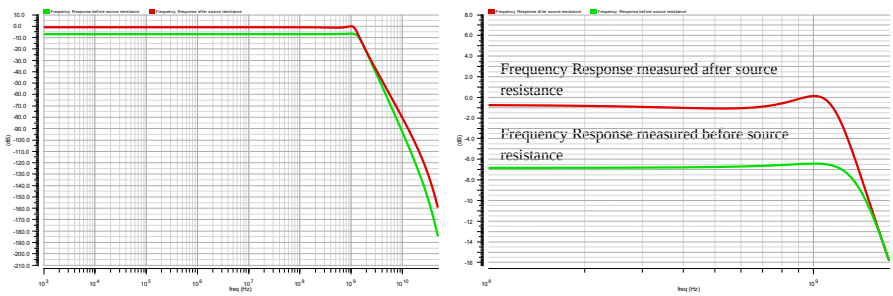

Fig. 44. Frequency response comparison at the different source point.

As explained in Tx case the ripples and different gain response in Fig. 44 is because of the transfer function measured from two different terminals of the source impedance.

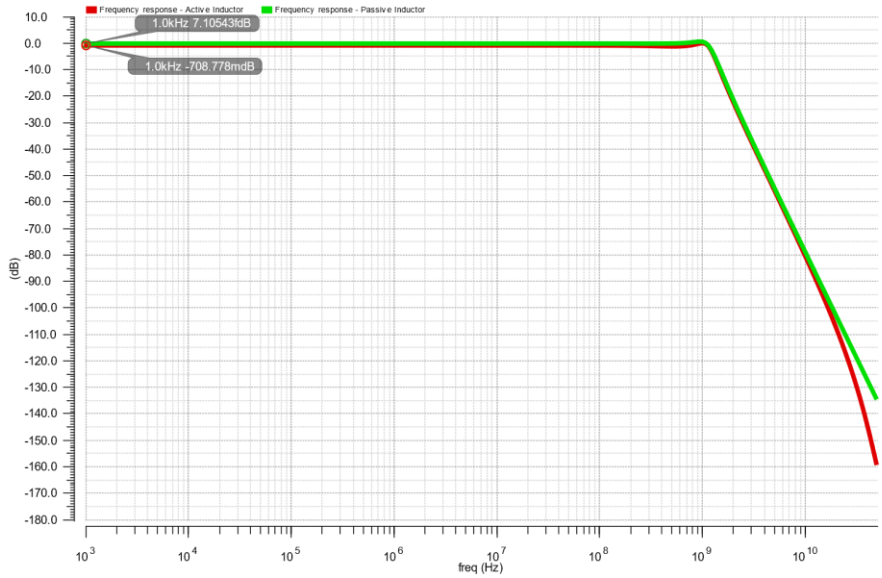

Fig. 45. The frequency response of the Gm-C filter versus ideal filter.

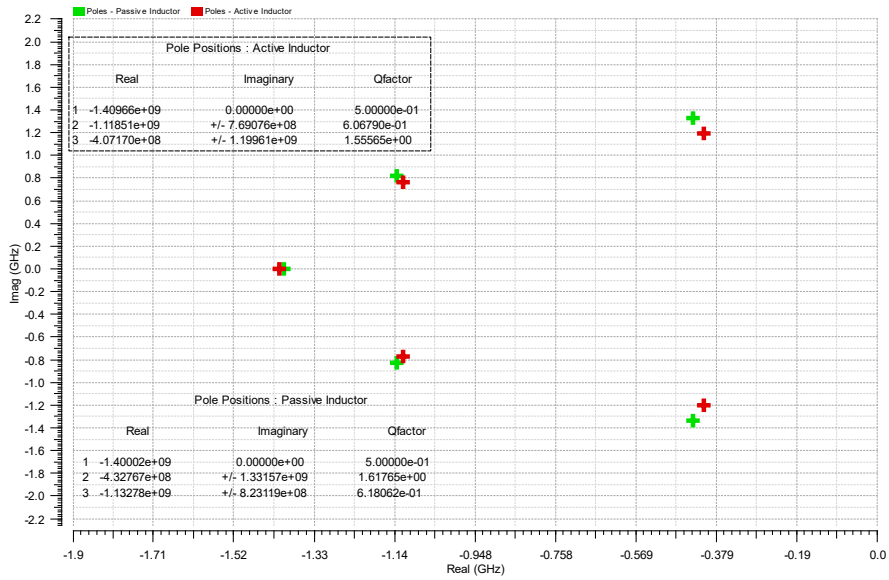

Fig. 46. The pole placements of the Gm-C filter versus ideal filter.

Both Rx and Tx cases have the same terminal impedances and this makes the response of Rx and Tx case to be identical and can be confirmed by comparing Fig. 40 & Fig. 41 along with Fig. 45 & Fig. 46.

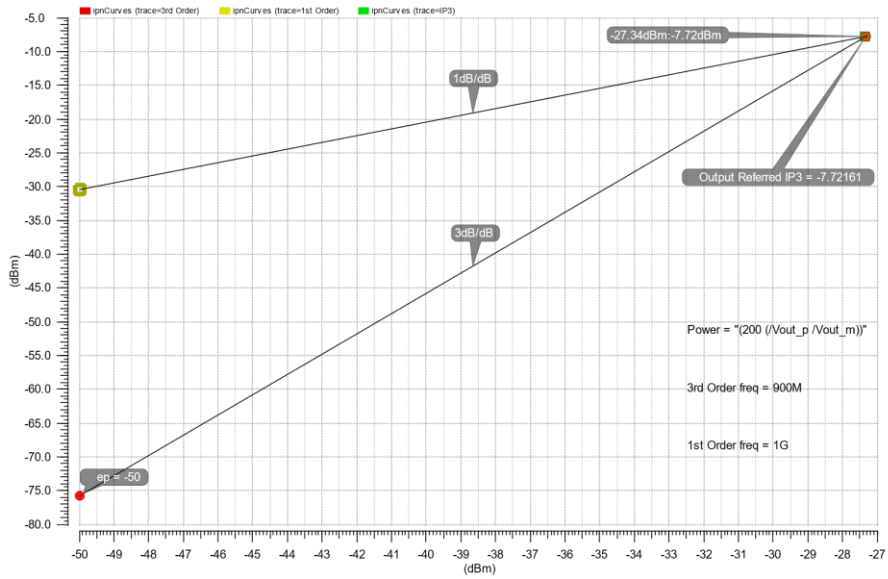

Fig. 47. Output referred IP3 of the Gm-C filter.

Table 14. Performance Parameters Rx.

PARAMETERS	***VALUES***
IDC	$9.598mA$
$IDC\_indctuctor1$	$4.827mA$
$IDC\_indctuctor2$	$4.771mA$
VCM	$408.4mV$
VCM_in	$403.9mV$
VCM_mid	$407.6mV$
VCM_out	$407.7mV$
Av_Gain_dB	$-0.7dB$
$1dB\ cutoff\ Frequency$	$1.186GHz$
$dB/Octave$	24.89
$Attenuation\ at\ 3.2GHz$	$32.45dB$

Table 14 shows the performance metric of the Rx case with parameter values close to the design specifications.

4. Mixer

Mixers are a three-port device that performs frequency translation by multiplying two signals. Fig. 48 shows the general mixer operation, it is seen from the illustration that the mixer adds (upconverts) and subtracts (down-converts) two signals in the frequency domain, as seen in Fig. 49 mixers are used for up-conversion of signal from baseband to radio frequency (RF) in the transmitter and down-conversion of signal from RF to baseband or intermediate frequency (IF) in the receiver chain. One input is for the information signal and the other is for the clock signal, the local oscillator (LO). Ideally, the signal at the output is the same as that at the information signal input, except shifted in frequency by an amount equal to the frequency of the LO. The mixer can be modeled as a simple multiplier that produces the product of inputs at the output in the time-domain or convolution of two signals in the frequency domain.

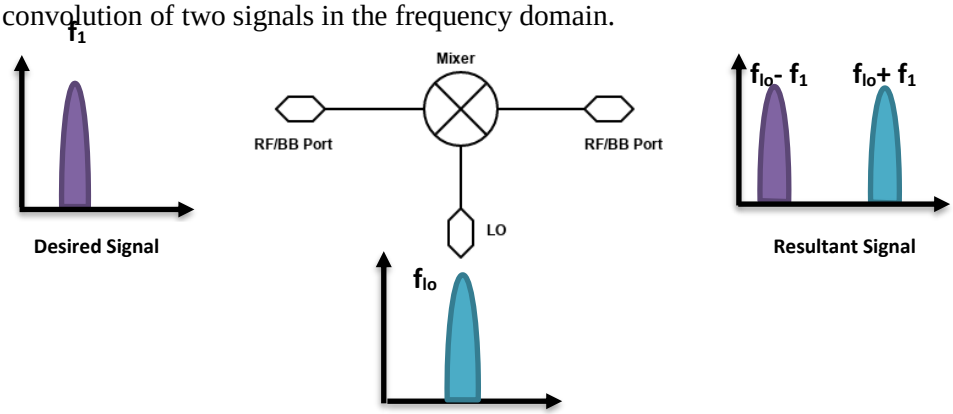

Fig. 48. Basic Operation of Frequency Mixer.

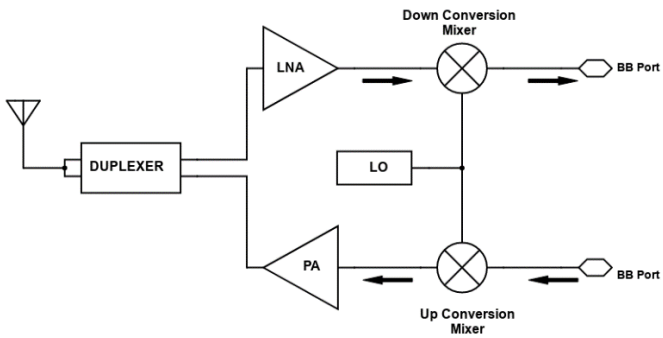

Fig. 49. Mixer in a Transceiver Chain.

4.1. Single Balanced and Double-Balanced Mixer

The simple single balanced mixer is sown in Fig. 50(a), it operates with a single-ended RF input and a single-ended LO. Thus, shown in Fig. 50(a) the switches are driven by LO phases thus commuting RF input to one of the outputs called a single balanced mixer, and thus proving a differential output reducing the complexity of the design. The single balanced mixer suffers from LO-RF and LO-IF feedthrough [10], LO-RF feedthrough can be effectively minimized if the circuit is perfectly symmetric.

To eliminate the effect of LO-IF feedthrough we connect two single balanced mixers such that the output LO feedthrough gets canceled, thus giving a new mixer topology called a double-balanced mixer as shown in Fig. 50(b).

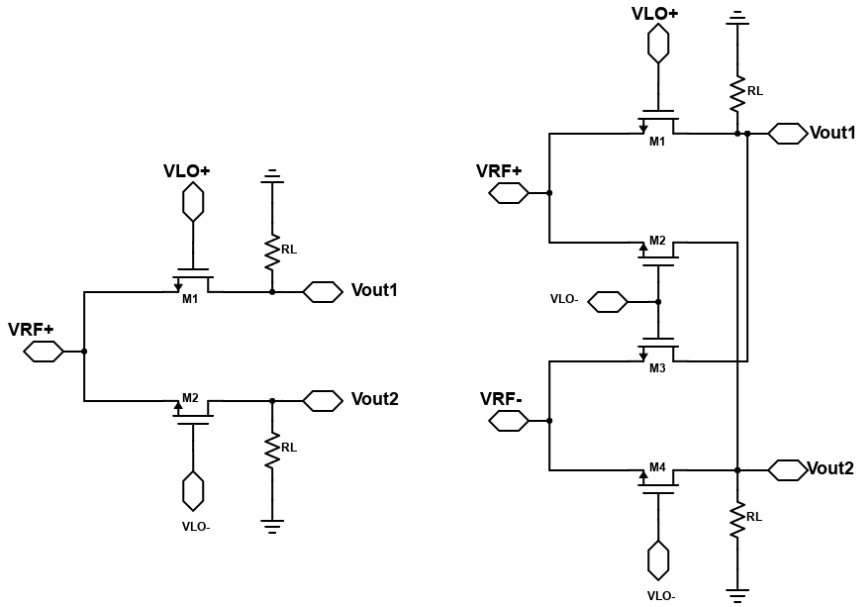

Fig. 50. Generic structure of (a) single and (b) double-balanced mixer.

4.2. Passive and Active Mixers

The mixers are broadly classified into passive and active topologies, each of which can be realized as a single or double balanced structure.

The passive mixer topology is one in which the transistor used do not act as an amplifying device they act just as switches to commute the signals. The conversion gain of the passive mixer is $20log(1/\pi) = -10dB$.

Active mixers are the ones which can be designed to have a conversion gain in one stage. Such mixers have three basic operations: conversion of RF voltage to current, steer the RF current by LO and convert the frequency-shifted signal back to voltage. The switching of signal from voltage to current and current to voltage helps to achieve higher gain. The conversion gain of an active mixer is $20log(^{2}/_{\pi}) \approx -4dB$.

4.3. I and Q Image Rejection Mixers

IQ and Image Reject (IR) or Single Sideband (SSB) mixers use similar circuitry to solve two different fundamental problems in communications and signal processing. IQ mixers address the problem of maximizing information transmission by allowing the user to modulate both the in-phase and quadrature components of a carrier simultaneously, thus multiplexing two signals onto the carrier. Image Reject mixers allow the user to select the desired signal in a crowded spectrum and suppressing the adjacent image signal, thus reducing the complexity in receiver filtering requirements.

An IQ mixer allows a system to send twice the information content in a double-sideband transmission without increasing bandwidth by utilizing 'quadrature' modulation. An IR mixer allows the selection of only one of either the LO + IF or the LO – IF frequencies while rejecting the other 'image' frequency.

4.4. IQ Mixer Operation and Structure

IR and Single Sideband performs similar operation on the signal, either as an up or a down converter. They use an IQ mixer as their core, with an extra IF quadrature hybrid coupler. The IQ mixer modulates both sidebands at the transmitter and then uses quadrature modulation to cancel one of the sidebands at the receiver, but an IR or SSB mixer uses a quadrature hybrid on the I and Q ports to cancel one of the sidebands at the mixer itself. Below Fig. 51 shows the block diagram of an IR/SSB mixer.

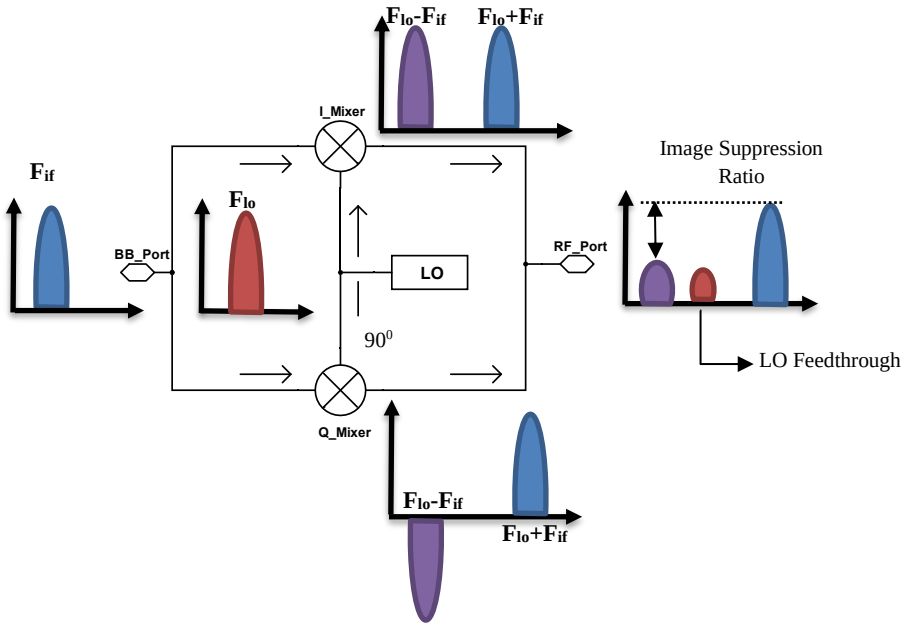

Fig. 51. Generic Structure of IQ Image Rejection Mixers.

For an IR mixer, this means that when a signal is down-converted from $f_{rf} = f_{lo} - f_{if}$ to f_{if}, any noise or spurious signals at $F = f_{lo} + f_{if}$ is rejected by an amount called the image rejection of the mixer. This amount, typically around $25\,dB$ for Image Reject mixers, is determined by the balance of the quadrature hybrids and mixer cores that make up the IR mixer.

There are several performance metrics to be considered when using an image reject mixer.

- *Image rejection levels:* The typical levels of image rejection that may be achieved are often in the region of $20 - 40\,dB$.
- *Conversion loss:* The conversion loss of an image rejection mixer will be higher than that of a standard mixer as the overall loss will need to include that of the quadrature hybrids, power splitters, etc. The additional loss introduced by these components will need to be added to the overall equation. However, the level of loss is still normally acceptable - typical figures expected maybe around $8 - 10\,dB$.
- *Frequency dependence:* The level of image rejection obtained with an image reject mixer is largely determined by the amplitude and phase balance within the image rejection mixer circuitry. These parameters are frequency-dependent to a degree

and therefore the performance of an image rejection mixer will also be frequency-dependent.

4.5. Bidirectional Mixer Topology

The proposed bidirectional IQ mixer is implemented as shown in Fig. 52, it consists of two double-balanced resistive mixers. The double-balanced mixer is composed of four NMOS transistors operating in the triode region.

The NMOS is operated as a resistive switch driven by the LO signal. The conversion loss of the doubly balanced resistive mixer is dominated by the on resistance of the switch, and the on-resistance of the NMOS is given by (40).

$$R_{on} = L \times \mu_n \times C_{ox} \times W\left[\left(V_{gs} - V_{th}\right) - V_{ds}\right], \tag{40}$$

where L is the length of the gate, μ_n is the electron mobility, C_{ox} is gate oxide capacitor per unit area, W is gate width, V_{th} is the threshold voltage, and V_{ds} is the drain-to-source voltage. Based on [9], the on-resistance can be reduced by increasing the device size and the dc gate bias voltage. However, the gate-to-source and gate-to-drain parasitic capacitances increase as the device size increases.

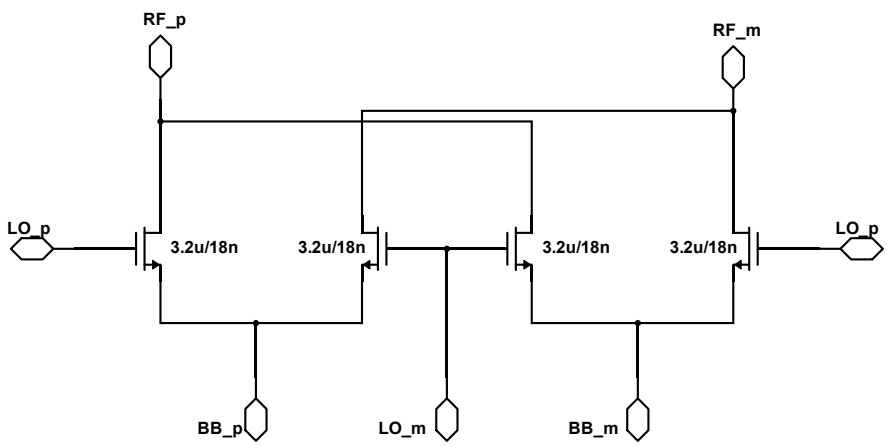

Fig. 52. Schematic of Passive Mixer.

The input impedance is an important parameter to measure since it affects the filter output and input terminations respectively in Tx and Rx

cases. The mixer input impedance is set to be differentially 200Ω by adjusting the W/L ratio of the transistors. Fig. 53 shows the measured input impedance value.

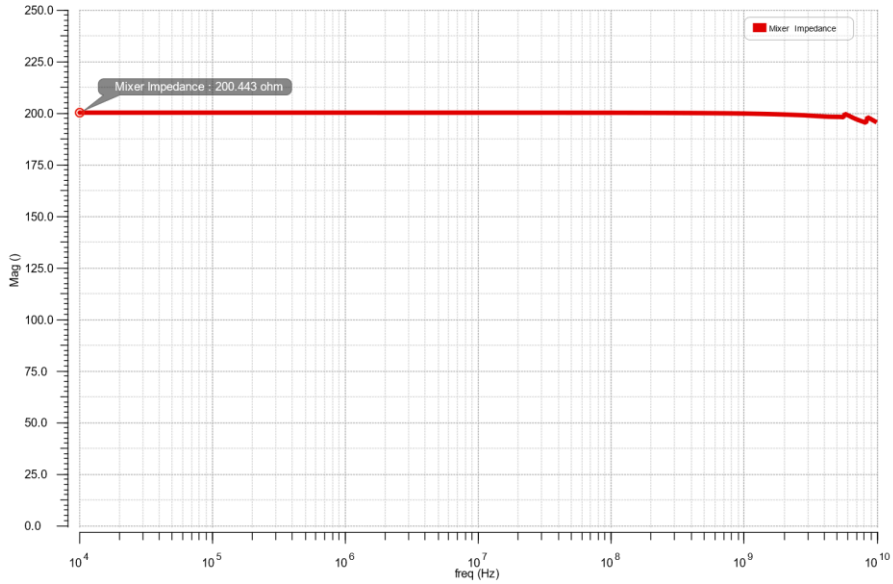

Fig. 53. Input Impedance of the Mixer.

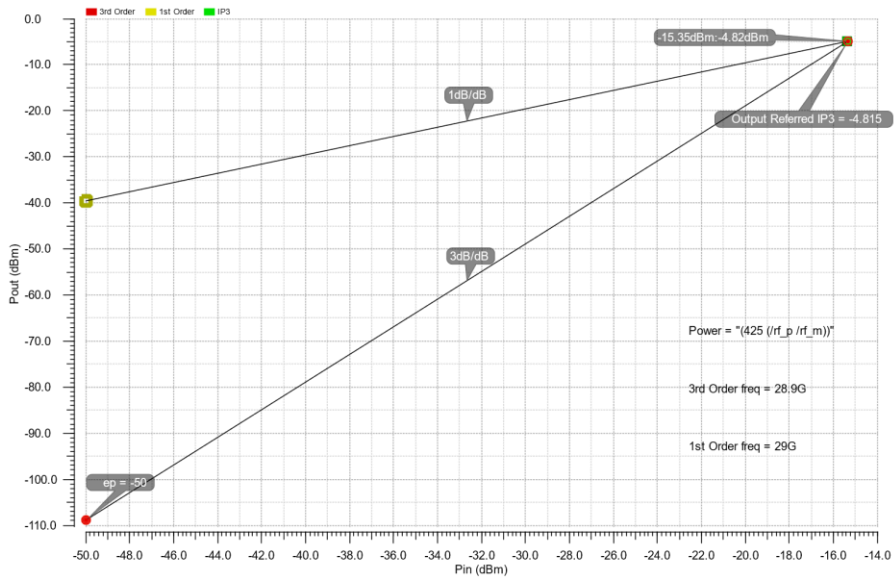

Fig. 54. Output referred IP3 of the Mixer.

5. Results

5.1. Top-Level Testbench Simulation

The bidirectional filter and mixer designed are integrated into a top-level test bench to measure the overall performance of the transceiver chain. The top-level testbench is designed as shown in Fig. 55, it contains baseband and RF stimuli/loads which are connected to filter and mixer respectively to model a complete transceiver chain.

5.1.1. Tx case

In the Tx chain, the baseband stimuli act as a voltage source to provide an in-phase differential signal for the I channel and 90° phase-shifted differential signals for the Q channel. The signals are band-limited by the LPF and up-converted by I and Q mixers respectively. The mixer is controlled by a 50% duty cycle LO as shown in Fig. 56. The output of IQ mixers is combined to suppress the image component and then passed through an LC resonator tuned at $28GHz$. The RF stimuli replicates input resistance of a power amplifier with a Rin of 425Ω differentially.

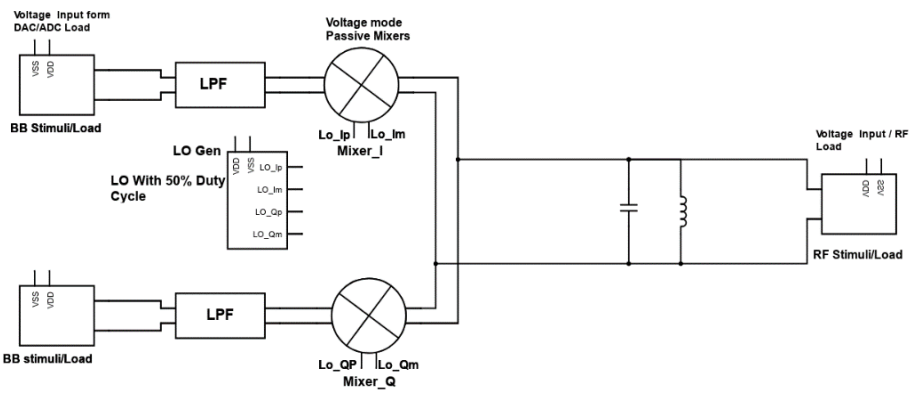

Fig. 55. Top-Level Schematic.

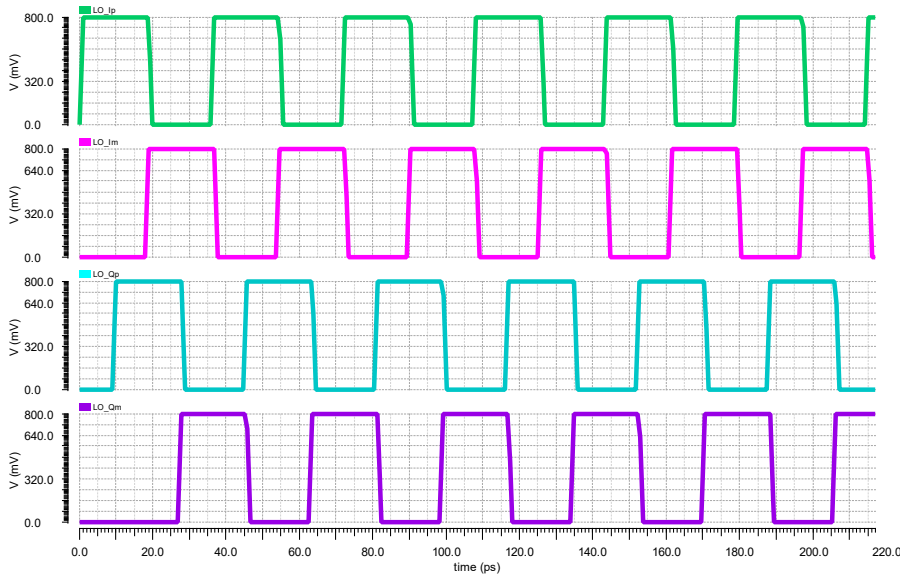

Fig. 56. LO Signal with 50% Duty Cycle.

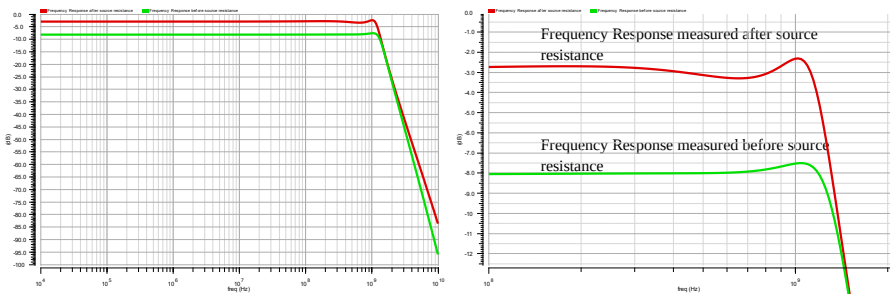

Fig. 57. Frequency response comparison at the different source point.

As explained in section 3.5.1, Fig. 57 shows the variation in voltage gain and presence of passband ripples, when the transfer function is measured at different source impedance terminals.

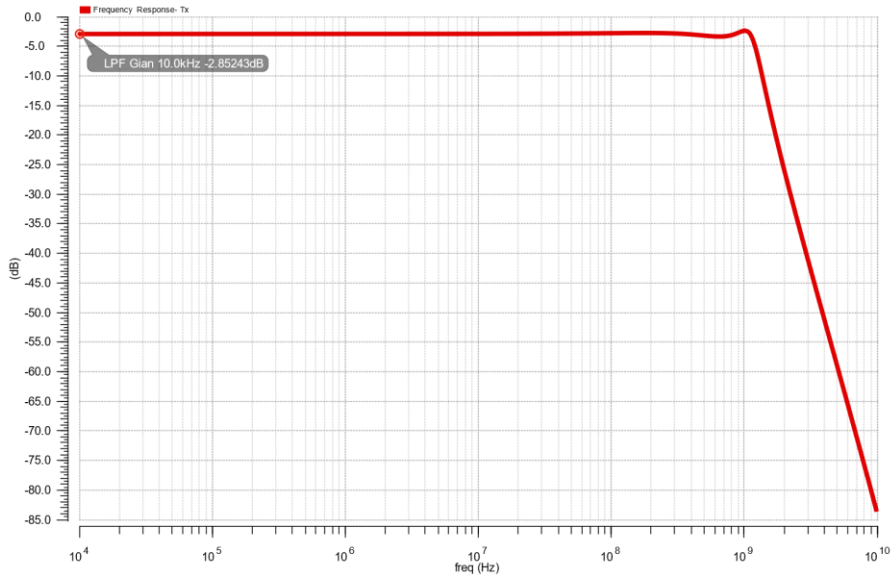

Fig. 58. Filter frequency response.

The frequency response of the filter measured from the output of the baseband block to the input of a mixer, as shown in Fig. 58, has $3dB$ loss as compared to measured results in 3.5.1. This loss in filter gain is because of parasitics from mixer integration.

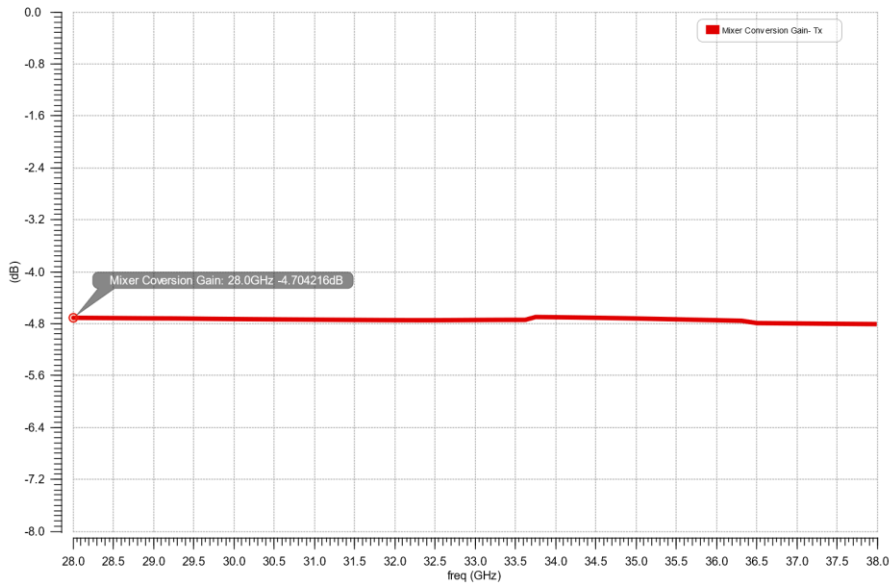

Fig. 59. Mixer conversion gain in dB.

Fig. 59 shows the conversion gain of the mixer and it is approximately $-4.7dB$ which is close to the theoretical value of $-4dB$.

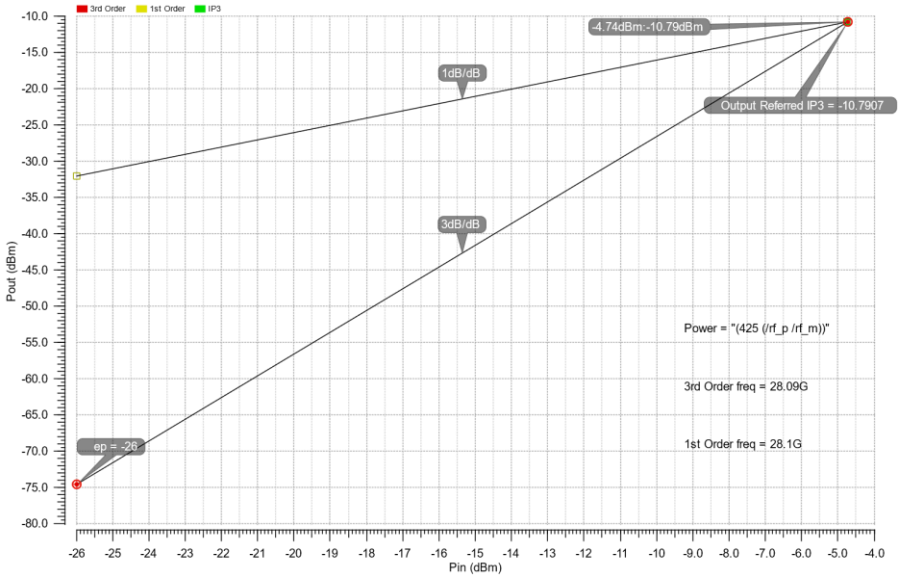

Fig. 60. Output referred IP3 in dBm.

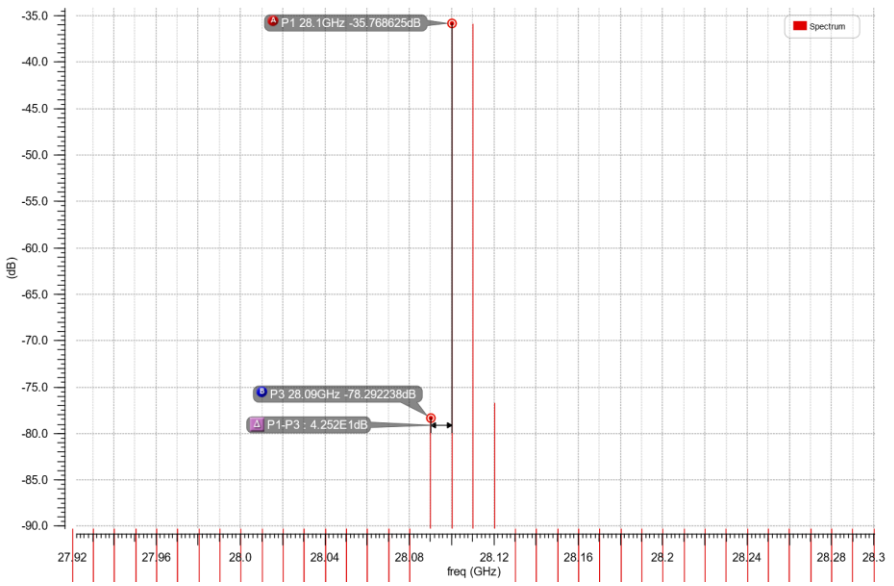

Fig. 61. Output spectrum in $dBVrms$ to calculate OIP3 in $dBVrms$.

The Output referred IP3 can be calculated using the spectrum values by the simple formula:

$$OIP3 = P1 + \frac{(P1 - P3)}{2} = -14.51dBV_{rms}$$

The above Fig. 60 and Fig. 61 shows the simulated values of OIP3 in dBm and $dBVrms$. As seen the system suffers from poor linearity. This might be due to the Gm-Cell topology, which is designed as a differential amplifier. We discuss methods to improve linearity further in chapter 7.

Table 15. Performance parameters.

PARAMETERS	***VALUES***
LDO_Vout_hb	$800mV$
LDO_Iout_hb	$22.92mA$
$IDC\_indctuctor1$	$5.82mA$
$IDC\_indctuctor2$	$5.583mA$
IDC_LPF	$11.4mA$
IDC_Mixer	0
VCM_LPF_DAC	$413.9mV$
VCM_LPF_MIX	$426.6mV$
VCM_in	$413.9mV$
VCM_mid	$426.5mV$
VCM_out	$426.6mV$
LO_{Ip}, Vpk	$515.2mV$
$Av\ LPF(hbac)$	$-2.852dB$
$Av\ Mixer(hbac)$	$-4.704dB$
$Av\ Overall(hbac)$	$-7.556dB$
$1dB\ cutoff\ Frequency$	$1.17GHz$
$dB/Octave$	24.88
$Attenuation\ at\ 3.2GHz$	$40.03dB$
$1st\ order\ harmonic$	$-35.77dBV_{rms}$
$3rd\ order\ harmonic$	$-78.29dBV_{rms}$
$Output\ referred\ TOI\ point\ in\ dBV_{rms}$	$-14.51dBV_{rms}$
$Output\ referred\ TOI\ point\ in\ dBm$	$-10.79dBm$
$Av\ LPF\ (hb)$	$-988.4mdB$
$Av\ Mixer(hb)$	$-4.761dB$
$Av\ Overall(hb)$	$-5.749dB$

Table 15 shows the simulation results of the Tx chain. The resulted values are close to the requirements. The overall current consumption of the Tx chain is $22.92mA$, which shows that power consumption is drastically reduced as compared to the existing architecture.

Output	Test	Min	Max	Mean	Median	Std Dev
LDO_Vout_hb	LPF_Tx	800m	800m	800m	800m	0
LDO_Iout_hb	LPF_Tx	21.24m	24.42m	22.88m	22.93m	690.2u
IDC_MIX	LPF_Tx	707.8a	707.8a	707.8a	707.8a	0
IDC_ind1	LPF_Tx	5.342m	6.285m	5.81m	5.826m	203.2u
IDC_ind2	LPF_Tx	5.237m	5.818m	5.57m	5.58m	135u
IDC_LPF	LPF_Tx	10.6m	12.09m	11.38m	11.41m	333.1u
Vcm_lpf_ad	LPF_Tx	403.9m	424m	414m	414m	4.245m
Vcm_lpf_mix	LPF_Tx	409.1m	443.4m	426.6m	426.1m	7.478m
VCM_in	LPF_Tx	403.9m	424m	414m	414m	4.245m
VCM_mid	LPF_Tx	406.9m	444.6m	426.5m	426.1m	7.635m
VCM_end	LPF_Tx	409.1m	443.4m	426.6m	426.1m	7.478m
LO_lp, Vpk	LPF_Tx	506.7m	515.2m	514.3m	515.2m	2.515m
Av_LPF_dB_V	LPF_Tx	-3.344	-2.498	-2.912	-2.904	199.4m
Av_Mix_dB_V	LPF_Tx	-5.228	-4.624	-4.883	-4.863	122.2m
Av_Overall_dB_V	LPF_Tx	-8.362	-7.396	-7.795	-7.754	201.4m
f3dB_V	LPF_Tx	1.121G	1.455G	1.233G	1.229G	58.89M
f1dB_V_	LPF_Tx	1.144G	1.5G	1.266G	1.263G	62.61M
Attn_3p2G_LPF_V	LPF_Tx	34.88	43.55	40.47	40.62	1.562
Attn_5G_LPF_V	LPF_Tx	50.85	59.19	56.15	56.35	1.521
Attn_10G_LPF_V	LPF_Tx	75.66	83.97	80.94	81.14	1.548
dB/Octave_V	LPF_Tx	24.38	25.15	24.79	24.79	171.2m
Zout	LPF_Tx	156.6	212.6	185.9	185.5	11.43

Fig. 62. Monte Carlo Results.

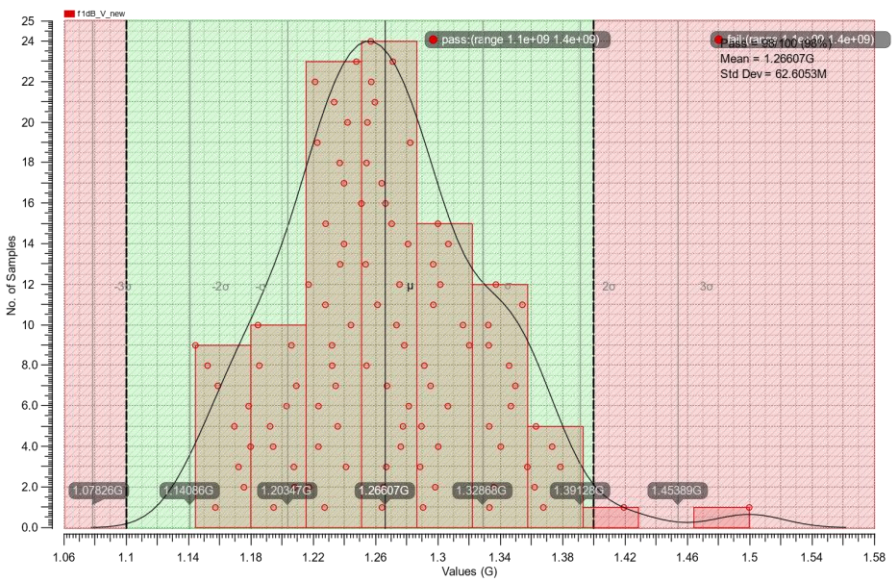

Fig. 63. 1dB cutoff frequency histogram.

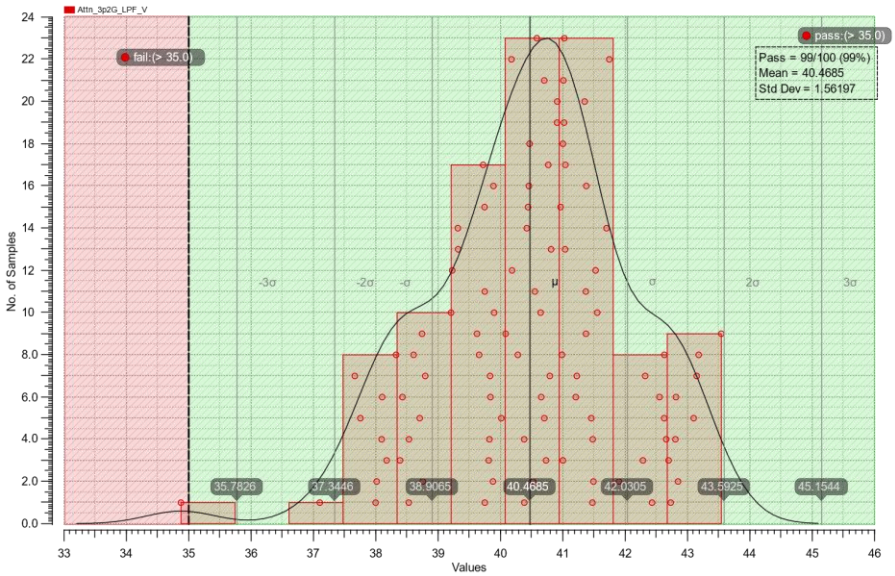

Fig. 64. Attenuation at 3.2GHz histogram.

The Monte Carlo simulations are run by varying the process parameter and mismatch to check the robustness of the system over a wide range of processes and temperature dependencies. Form Fig. 62 it is seen that the system remains stable for PVT variations and Fig. 63 and Fig. 64 show the histogram of $1dB$ cutoff frequency with a deviation of $62MHz$ and attenuation at $3.2GHz$ with a deviation of 1.5 from nominal values.

5.1.2. Rx case

In the Rx chain, the baseband stimuli act as a load as seen from ADC input which is differentially 200Ω. The signal source is provided by RF stimuli which gives differential voltage input, the signals are down converted by I and Q mixers respectively. The outputs of I/Q mixers are forwarded to the LPF filters to remove any high-frequency components.

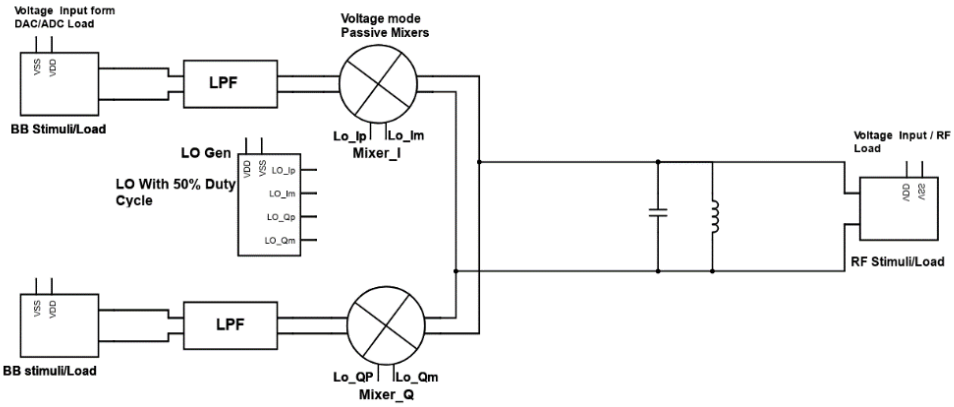

Fig. 65. Top-Level Schematic.

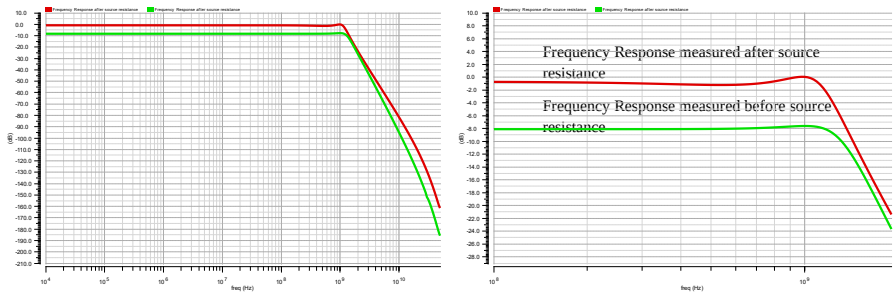

Fig. 66. Frequency response comparison at the different source point.

In the Rx case, the input for the filter is from the mixer and the input impedance is seen from the output resistance of mixer transistors, as explained in the previous chapter the transfer function is measured from different source impedance terminals, and Fig. 66 shows the effect of measuring filter response at different source impedance terminals.

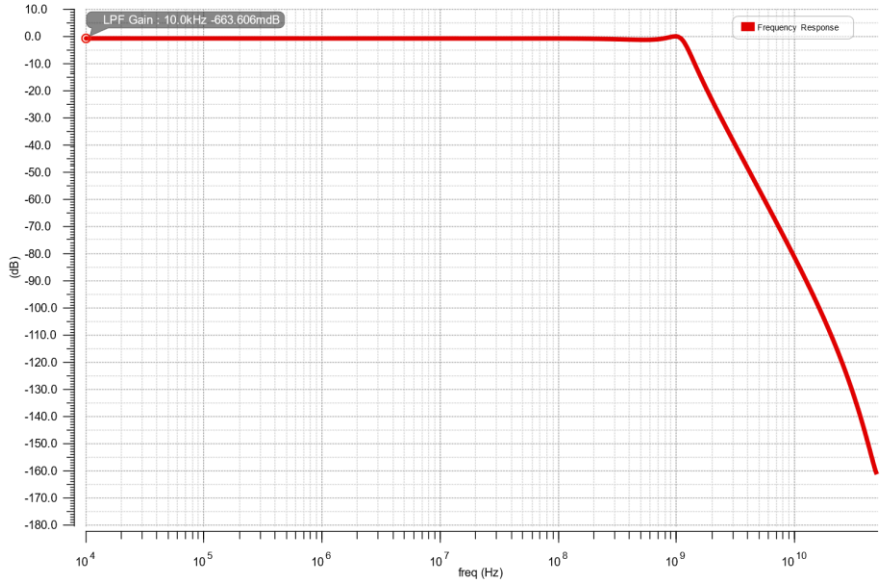

Fig. 67. Filter frequency response.

The frequency response of the filter measured from the mixer output to the input of a baseband load is shown in Fig. 67. The filters have a similar response as compared to measured results in 3.5.2.

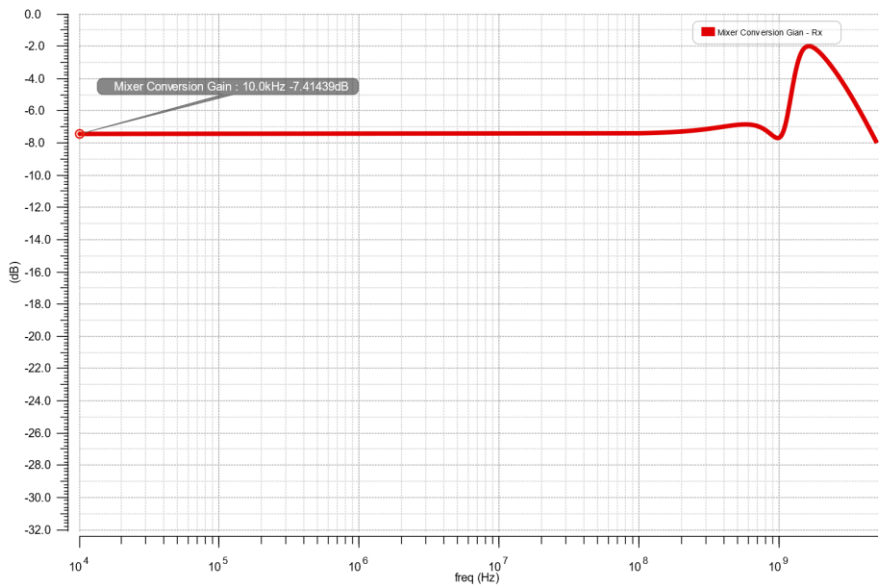

Fig. 68. Mixer conversion gain in dB.

Fig. 68 shows the conversion gain of the mixer and it is approximately $-7.4dB$. Theoretical calculation gives $-4dB$ but the signal splits into half at the input of IQ mixer resulting in an additional $3dB$ loss.

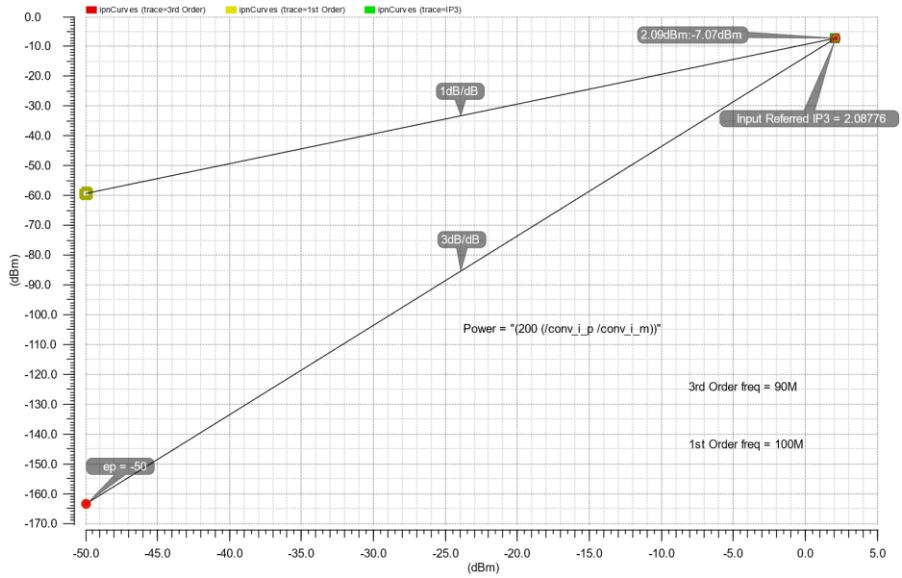

Fig. 69. Input referred IP3 in dBm.

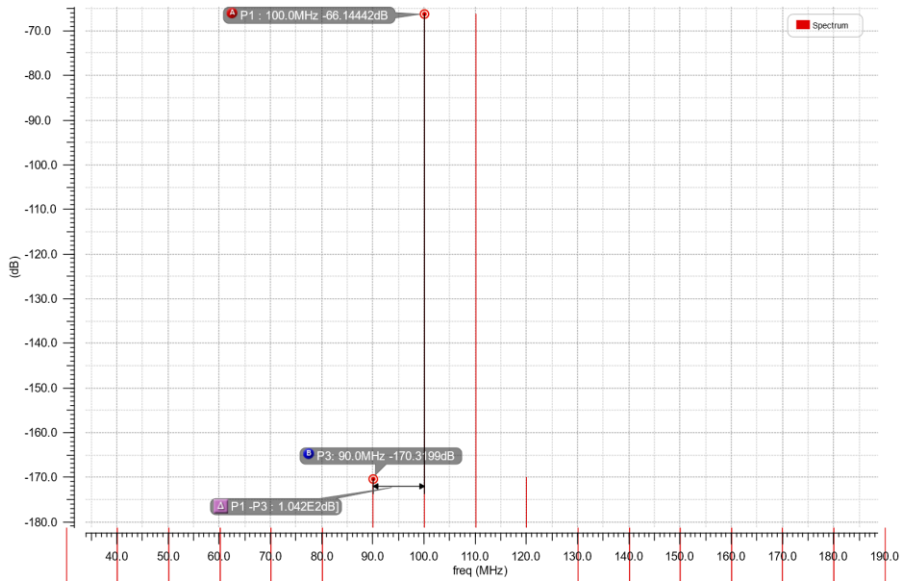

Fig. 70. Output spectrum in $dBVrms$ to calculate OIP3 in $dBVrms$.

$$OIP3 = P1 + \frac{(P1 - P3)}{2} = -14.06dBVrms$$

The simulated values of IIP3 in dBm and OIP3 in $dBVrms$ for Rx case is shown in Fig. 69 and Fig. 70, as seen from Tx case the system suffers from poor linearity in Rx mode of operation as well, this might be due to the Gm-Cell structure designed using a differential amplifier, the methods to improve linearity is discussed in chapter 7.

Table 16. Performance parameters.

PARAMETERS	***VALUES***
LDO_Vout_hb	$800mV$
LDO_Iout_hb	$22.28mA$
$IDC\_indctuctor1$	$5.581mA$
$IDC\_indctuctor2$	$5.581mA$
IDC_LPF	$11.16mA$
IDC_Mixer	0
VCM_LPF_ADC	$426.6mV$
VCM_LPF_MIX	$426.6mV$
VCM_{in}	$426.6mV$
VCM_mid	$426.6mV$
VCM_out	$426.6mV$
LO_{Ip}, Vpk	$515.2mV$
$Av\ LPF(hbac)$	$-663.6mdB$
$Av\ Mixer(hbac)$	$-7.414dB$
$Av\ Overall(hbac)$	$-8.078dB$
$1dB\ cutoff\ Frequency$	$1.149GHz$
$dB/Octave$	25
$Attenuation\ at\ 3.2GHz$	$39.64dB$
$1st\ order\ harmonic$	$-66.14dBV_{rms}$
$3rd\ order\ harmonic$	$-170.3dBV_{rms}$
$Output\ referred\ TOI\ point\ in\ dBV_{rms}$	$-14.06dBV_{rms}$
$Input\ referred\ TOI\ point\ in\ dBm$	$2.08dBm$
$Av\ LPF\ (hb)$	$-702.1mdB$
$Av\ Mixer(hb)$	$-7.383dB$
$Av\ Overall(hb)$	$-8.085dB$

Table 16 shows the performance metric of the Rx chain and the parameter values are around the desirable range. The overall power consumption of the Rx chain is $22.28mA$, which shows that power consumption is drastically reduced by adopting bidirectional topology.

Test	Output	Min	Max	Mean	Median	Std Dev
LPF_Rx	LDO_Vout_hb	800m	800m	800m	800m	0
LPF_Rx	LDO_Iout_hb	20.77m	23.56m	22.24m	22.29m	618.9u
LPF_Rx	IDC_MIX	-713.3a	-705a	-708.4a	-707.8a	3.063a
LPF_Rx	IDC_LPF	10.45m	11.65m	11.14m	11.16m	273.5u
LPF_Rx	IDC_ind1	5.212m	5.851m	5.569m	5.579m	140.5u
LPF_Rx	IDC_ind2	5.235m	5.817m	5.569m	5.579m	135.2u
LPF_Rx	Vcm_lpf_ad	408m	443.9m	426.6m	426.5m	7.588m
LPF_Rx	Vcm_lpf_mix	406.2m	443m	426.6m	426m	7.776m
LPF_Rx	VCM_in	408m	443.9m	426.6m	426.5m	7.588m
LPF_Rx	VCM_mid	406.9m	444.6m	426.6m	426.2m	7.639m
LPF_Rx	VCM_end	409.1m	443.4m	426.6m	426.1m	7.477m
LPF_Rx	LO_Ip, Vpk	515.2m	515.2m	515.2m	515.2m	0
LPF_Rx	Av_Mixer_dB_V	-8.032	-6.987	-7.537	-7.508	190.6m
LPF_Rx	Av_LPF_dB_V	-952.1m	-348.8m	-660.5m	-675.6m	135.1m
LPF_Rx	Av_Overall_dB_V	-8.837	-7.783	-8.198	-8.172	202.7m
LPF_Rx	F1dB_V	510.7M	1.345G	1.143G	1.142G	84.21M
LPF_Rx	Attn_3p2G_LPF_v	34.45	42.83	39.7	39.86	1.578
LPF_Rx	Attn_5G_LPF_v	50.51	58.53	55.53	55.71	1.528
LPF_Rx	Attn_10G_LPF_v	75.54	83.6	80.52	80.74	1.54
LPF_Rx	dB/Octave_v	24.77	25.24	24.99	24.99	86.93m

Fig. 71. Monte Carlo results.

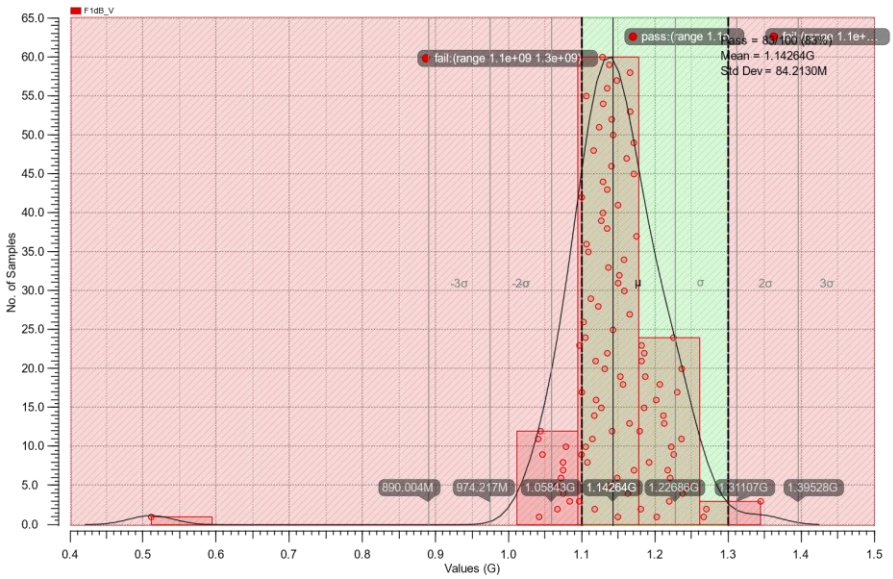

Fig. 72. 1dB cutoff frequency Histogram.

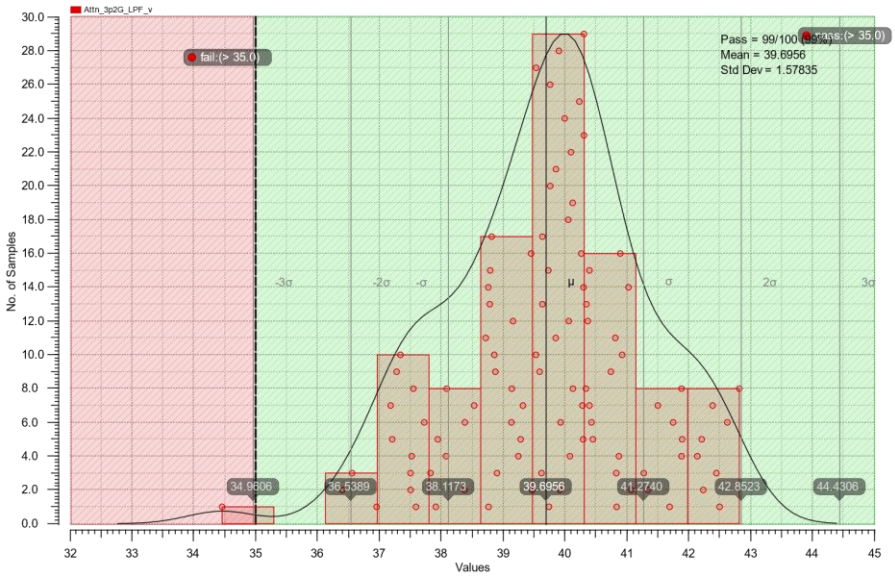

Fig. 73. Attenuation at 3.2GHz Histogram.

The Monte Carlo simulations are run by varying the process parameter and temperature to check the robustness of the system over a wide range of processes and temperature dependencies. Form Fig. 71 it is seen that the system remains stable for PVT variations and Fig. 72 and Fig. 73 show the histogram of $1dB$ cutoff frequency with a deviation of $84MHz$ and attenuation at 3.2GHz with a deviation of 1.5 from nominal values.

6. Conclusions

The primary purpose of this thesis is to investigate the bi-directional filter and mixer topology combination for the transceiver chain in 5G TDD Architecture. The study of different bidirectional filter topologies showed that the Gm-C-based structure has better performance over the desired frequency range. The simulated results also show that the Low Pass Filter(LPF) using Gm-C cell has good bi-directional behavior and has a sharp roll-off at $1.2GHz$ and the desired attenuation of $40dB$ at $3.2GHz$. The mixer was designed using a transistor implementation of diode ring topology which is bi-directional and operated as a passive mode voltage mixer. On comparing the simulated result with existing architecture for 5G mm-Wave high band, the pull-up effect on Voltage Controlled Oscillator(VCO) for switching between Tx and Rx cases separately is eliminated by adapting a single mixer block for both the mode of operation which will account for low power consumption and also reduces the routing complexity of Local Oscillator(LO) signals to the mixer block in layouts. Since we are using the same hardware blocks for Tx and Rx mode of operation there is a considerable reduction in the area as well. Therefore, the results prove that Gm-C based architecture seems promising for achieving a bidirectional filter with a good performance metric. Nevertheless, some linearity issues can be effectively corrected using different Gm cell structures.

7. Future work

- Bidirectional LNA and PA: In addition to the bi-directional LPF and mixer, RF front end LNA and PA can also be made bidirectional [12] and combined to make the overall transceiver chain compact. Research and development of this module must be carried out.
- Linearity Improvement: In the Gm-C inductor designed filter linearity is an issue. Modern techniques must be employed to improve linearity[1].
- Comparison with other filter and mixer topologies: Active inductors can be implemented in many ways and topologies. One of them is Wu's Inductor [11]. It will be intuitive to compare different filters and mixer topologies combinations for better performance, and reliability.

References

[1] Rolf Schaumann, Haiqiao Xiao, and Van Valkenburg Mac, "*Design of Analog filters (2nd. ed.)*." USA, Oxford University Press, Inc., 978-0195373943, 2009.

[2] Pactitis, "*Active Filters: Theory and Design*" USA, CRC Press., 978-1420054774, 2018.

[3] Mihai, Bogdan & Mihai, Panu. (2015). LabVIEW Modeling and Simulation of The Digital Filters. 10.13140/RG.2.1.2567.6641.

[4] https://en.wikipedia.org/wiki/Butterworth_filter.html

[5] https://www.electronics-tutorials.ws/filter/filter_8.html

[6] Li Tan, Jean Jiang, in Digital Signal Processing (Second Edition), 2013.

[7] Tellegen BDH. Passive Four Terminal Network for Gyrating a Current into a Voltage. Google Patents 2,647,239. 1953.

[8] S. Weng, C. Shen, and H. Chang, "A wide modulation bandwidth bidirectional CMOS IQ modulator/demodulator for microwave and millimeter-wave gigabit applications," 2012 7th European Microwave Integrated Circuit Conference, Amsterdam, 2012, pp. 8-11.

[9] Brahim Bensalem, James T. Aberle, "A New High-Speed Memory Interconnect Architecture Using Microwave Interconnects and Multicarrier Signaling", *Components Packaging and Manufacturing Technology IEEE Transactions on*, vol. 4, no. 2, pp. 332-340, 2014.

[10] *Behzad Razavi. 2011. RF Microelectronics (2nd Edition) (Prentice Hall Communications Engineering and Emerging Technologies Series) (2nd. ed.). Prentice-Hall Press, USA.*

[11] Chia-Hsin Wu, Jieh-Wei Liao, and Shen-Iuan Liu, "A 1V 4.2mW fully integrated 2.5Gb/s CMOS limiting amplifier using folded active inductors," 2004 IEEE International Symposium on Circuits and Systems (IEEE Cat. No.04CH37512), Vancouver, BC, 2004, pp. I-1044.

[12] J. Pang et al., "21.1 A 28GHz CMOS Phased-Array Beamformer Utilizing Neutralized Bi-Directional Technique Supporting dual-polarized MIMO for 5G NR," 2019 IEEE International Solid-State Circuits Conference - (ISSCC), San Francisco, CA, USA, 2019, pp. 344-346.

[13] CC BY-SA 3.0, https://en.wikipedia.org/w/index.php?curid=3458784